Similarity Parameter Evolution within a Magnetic Nozzle with Applications to Laboratory Plasmas

IEPC-2011-229

Presented at the 32nd International Electric Propulsion Conference,
Wiesbaden, Germany
September 11–15, 2011

Justin M. Little* and Aaron S. Rubin † and Edgar Y. Choueiri ‡
Princeton University, Princeton, New Jersey, 08540, USA

The scaling of plasma confinement, acceleration, and detachment from a magnetic nozzle is investigated within the context of present laboratory experiments. A review of the similarity parameters relevant to magnetic nozzle plasmas is provided. A quasi-one-dimensional model of the expanding plasma is then used to determine the evolution of these parameters downstream from the nozzle throat. Two types of plasmas are considered using this model: a cold ion, hot electron plasma with varying degrees of electron cooling; and a hot ion, cold electron plasma with varying degrees of ion temperature anisotropy. Finally, the results of the model are applied to ten different magnetic nozzle experiments to determine their relevant physical regimes.

I. Introduction

Simply stated, magnetic nozzles convert the thermal energy of a plasma into directed kinetic energy. This conversion is achieved by means of a strong convergent-divergent magnetic field contoured similarly to the solid walls of a conventional de Laval nozzle.[1] The applied field, typically formed using permanent magnets or electromagnetic coils, confines the plasma and acts as an effective "magnetic wall" through which the thermal plasma expands. Momentum is transmitted from the expanding plasma to the thruster by the interaction between induced plasma currents and currents within the applied field circuit.[2] Applications include laboratory simulations of space plasmas,[3] surface processing,[4] and plasma propulsion for spaceflight.[5–7]

The mechanism by which ions are accelerated is fundamental to the understanding of magnetic nozzles for propulsion applications as the majority of kinetic energy within the exhaust plume is carried by the ions by virtue of their mass. In a conventional de Laval nozzle, a pressure gradient accelerates the largely neutral, subsonic propellant gas through the convergent section of the nozzle to a sonic condition at the throat. The divergent section of the nozzle provides further acceleration of the now supersonic flow. This idealized picture is sufficient to describe ion acceleration through the convergent-divergent magnetic field topology in a magnetic nozzle in the limit of cold electrons and thermally isotropic ions ($T_e << T_{i,\parallel} = T_{i,\perp}$).[1] Multiple deviations from this idealized picture exist, however, due to the complex nature of plasmas.

The nature of the plasma prior to expansion through the magnetic nozzle depends on the plasma source and heating mechanism. Energy may be deposited into the thermal motion of either electrons, ions, or both species. Furthermore, this energy may specifically target motion in either the parallel or perpendicular direction with respect to the applied magnetic field. Depending on the collisional and confinement timescales, significant temperature anisotropies ($T_{i,\parallel} \neq T_{i,\perp}$) and species non-equilibrium ($T_e \neq T_i$) effects may alter the means by which ions are accelerated through the magnetic nozzle. A detailed description of the different ion acceleration mechanisms is included in Section II.B.

The feasibility of using plasma flow along magnetic fields to produce thrust has been questioned due to the tendency of the highly conductive plasma to remain tied to necessarily closed magnetic field lines.

*Graduate Research Assistant, Mechanical and Aerospace Engineering, jml@princeton.edu.
†Graduate Research Assistant, Mechanical and Aerospace Engineering.
‡Chief Scientist, EPPDyL; Professor, Applied Physics Group, Mechanical and Aerospace Engineering.

Efficient detachment of the plasma from the magnetic nozzle is paramount for space propulsion applications. As such, recent experimental, theoretical, and computational research in magnetic nozzles has focused, to much debate, on plasma detachment. Detachment through resistive diffusion, demagnetization, and induced magnetic fields are among the leading theories by which the plasma may detach. Section II.C. describes each detachment mechanism in more detail.

In light of all the complex physical processes that may occur within magnetic nozzle plasmas, the main goal of this paper is to review the fundamental physics associated with plasma acceleration and detachment, and determine for the first time the scaling of these physics throughout the expanding plasma. We begin with a review of the similarity parameters that properly characterize magnetic nozzle plasmas. We then use a quasi-one-dimensional description of the expanding plasma to determine the evolution of these parameters throughout the exhaust plume. Using these results, we compare the timescales associated with multiple physical processes to the plasma confinement time, and arrive at method to determine the relevant acceleration and detachment processes. Finally, we conclude with a review of past and present magnetic nozzle experiments within the context of plasma acceleration and detachment.

An exhaustive analysis of the influence each physical regime has on the efficiency of the nozzle is beyond the scope of this work. Furthermore, our omission of non-ideal processes related to kinetic effects, turbulent transport, and electromagnetic instabilities should not be equated with their insignificance within magnetic nozzle plasmas. On the contrary, any proper treatment of plasma expansion through a magnetic nozzle will likely need to include these effects. With that said, analytic results of sufficient transparency have yet to reveal themselves to decades worth of high-level research into these phenomena, thus their inclusion must be left for future studies.

II. Magnetic Nozzle Physics

With the goal of understanding the physical regimes for the diffent acceleration and detachment mechanisms, we proceed now with an in-depth review of the dimensionless parameters relevant to magnetic nozzle flows. Three general regions of the magnetic nozzle plasma are considered: the plasma source, acceleration region, and detachment region. This division, while useful for organization, should not imply that the physics within each region have limited influence on the others.

It should be noted that all of the equations given within this section are for quantities represented in SI units (mks), with the exception of temperatures, which should be expressed in terms of electron volts.

A. Plasma Source

The plasma source is considered as the location where the propellant is ionized and subsequently heated. It is analogous to the combustion chamber of a conventional nozzle. Important characteristics of the plasma within this region and its quality, confinement, and stability.

1. Plasma Quality

We refer to the plasma quality as how well the ionized propellant is represented by the classical theoretical description of a plasma. Furthermore, the criteria for portraying the plasma as a continuum as opposed to a Knudsen gas is included within this description.

One of the most fundamental properties of a plasma is its ability to shield electrical charges within itself. The characteristic length over which this shielding occurs is referred to as the Debye length, λ_D.[8] It is necessary to have this length be much smaller than the dimensions of the plasma. The normalized Debye length is given by the following expression,

$$l_D \equiv \frac{\lambda_D}{r_p} \approx 7.4 \times 10^3 \frac{1}{r_p n^{1/2}} \left(\frac{T_e T_i}{T_e + T_i} \right)^{1/2}. \tag{1}$$

Here, r_p is the plasma radius, T_e is the electron temperature, T_i is the ion temperature, and n is the plasma density.. Proper shielding requires $l_D << 1$.

It is also critical to have enough charge carriers within the volume spanned by the Debye length, or Debye sphere. The approximate number of charged particles within this volume is represented by the

plasma parameter,[8]

$$\Lambda_p \equiv n\lambda_D^3 \approx 4.1 \times 10^{11} \frac{1}{n^{1/2}} \left(\frac{T_e T_i}{T_e + T_i} \right)^{3/2}, \tag{2}$$

with the requirement of $\Lambda_p >> 1$ necessary to fulfill the statistical description of a plasma.

The Knudsen number is defined as the ratio of the collisional mean free path, λ_{mfp}, of a particle to the length scale of the physical system. It essentially indicates how well a fluid description applies to a given gas.[9] The Knudsen numbers for electrons and ions are:

$$Kn_e \equiv \frac{\lambda_{mfp,e}}{r_p} \approx 5.9 \times 10^5 \frac{T_e^{1/2}}{r_p} \left(\sum_j \nu_{ej} \right)^{-1}, \tag{3}$$

$$Kn_i \equiv \frac{\lambda_{mfp,i}}{r_p} \approx 1.4 \times 10^4 \frac{T_i^{1/2}}{r_p \mu_i^{1/2}} \left(\sum_j \nu_{ij} \right)^{-1}. \tag{4}$$

The atomic weight of the ions is denoted by μ_i, while the subscript j represents the sum over all species present within the plasma. A species may be accurately described as a fluid if $Kn << 1$. On the other hand, a kinetic description of the species should be used for $Kn > 1$.

2. Confinement

The dimensionless parameters within this section describe the efficacy of plasma confinement by the applied magnetic field within the source. Furthermore, the influence of the plasma on the applied magnetic field is considered.

The most basic requirement for magnetic confinement of a plasma is that the Larmor radius associated with the orbit of the particles be much smaller than the scale length of the plasma.[8] The normalized electron and ion Larmor radii are given as follows,

$$l_e \equiv \frac{r_{L,e}}{r_p} \approx 2.4 \times 10^{-6} \frac{T_e^{1/2}}{r_p B}, \tag{5}$$

$$l_i \equiv \frac{r_{L,i}}{r_p} \approx 1.0 \times 10^{-4} \frac{\left(\mu_i T_{i\perp,0}\right)^{1/2}}{r_p B}, \tag{6}$$

where the magnetic field strength is given by B. Confinement of each species is only possible if its respective normalized Larmor radius is less than unity.

Sometimes the case arises for which $l_e < 1 < l_i$. While the ions are not strictly bound to the magnetic field, ion confinement is still achieved by a potential well that develops due to the tendency of the plasma to remain quasi-neutral.

The diamagnetic nature of plasma may also lead to significant perturbations to the applied magnetic field within the plasma source. The strength of these perturbations depends on the ratio of the thermal to magnetic energies of the plasma.[8] This parameter, referred to as the thermal-beta, may be found from

$$\beta_p \equiv \frac{2p}{B^2/\mu_0} \approx 4.0 \times 10^{-25} \frac{n}{B^2} \sum_j T_j, \tag{7}$$

Typically, induced field effects manifest for $\beta_p > 10^{-2}$. As β_p approaches unity, an unmagnetized plasma core develops within a magnetized current layer, and induced magnetic fields must be included in any analysis. However, for $\beta_p < 10^{-2}$ only the applied field influences the behavior of the plasma.

Resistive diffusion of the magnetic field into a high-β plasma may also influence the nature of the magnetic nozzle plasma source. The extent of this diffusion is represented by the magnetic Reynolds number, or

$$Re_M \equiv \frac{\mu_0 L V}{\eta} \approx 8.8 r_p T_e^{3/2} \left(\frac{\gamma_e T_e + 3T_{i,\parallel}}{\mu_i} \right)^{1/2} \tag{8}$$

In the equation above we have taken the characteristic length, L, and characteristic velocity, V, as the plasma radius and parallel ion sound speed, respectively. Furthermore, the Spitzer cross-field resistivity is used for

η.[8] Essentially, the magnetic Reynolds number relates the relative strength of magnetic field convection as compared to magnetic field diffusion. For $Re_M << 1$, the resistivity of the plasma is large enough to allow a substantial diffusion layer to develop at the plasma-vacuum interface.

3. Stability

Stability of the plasma source may also play a crucial role in the performance of a magnetic nozzle. The importance of instabilities may be quantified by comparing the growth rate of the strongest instability with the rate at which plasma exits the source region. If the former rate is much greater than the latter, the efficiency of the plasma source may drastically decrease, and extinction of the plasma may results. Further characterization of plasma stability will likely depend strongly on the nature of the specific plasma source, and is beyond the scope of this work.

B. Acceleration Region

Similar to a conventional de-Laval nozzle, acceleration in a magnetic nozzle occurs in the convergent-divergent section of the applied magnetic topology. Deviations from the ideal model of isentropic expansion may occur due to a variety of reasons. In this section, we concentrate on the non-dimensional parameters that describe the effects of thermal anisotropies, species non-equilibrium, and ionization and recombination.

1. Temperature Isotropy

A number of methods may be used to heat the ions within a plasma. Two such methods are ion cyclotron resonance heating (ICRH)[10] and heating with beating electrostatic waves (BWX).[11,12] Many of these concepts require strong guiding magnetic fields, which may lead to regimes where the collision time is long compared to the ion gyroperiod but short compared to the equilibration time between the ion parallel and perpendicular temperatures. The result is an anisotropic plasma with $T_{i,\parallel} \neq T_{i,\perp}$. If significant anisotropies are present within the plasma, acceleration manifests from the conservation of the first adiabatic invariant, or magnetic mirror force. Acceleration in an isotropic plasma, on the other hand, is purely thermal.[13]

The strong magnetic fields associated with a number of plasma sources and heating mechanisms may lead to significant anisotropies within the plasma. We begin by defining the degree of ion thermal isotropy as,

$$\Theta_{iso} \equiv \frac{T_\perp}{T_\parallel}, \tag{9}$$

where $T_\perp$ and $T_\parallel$ are the ion temperatures parallel and perpendicular to the magnetic field vector, respectively. A thermally isotropic plasma will have $\Theta_{iso} = 1$. We should note here that electron temperature anisotropies will not be included in the subsequent analysis due to the fact that the electron temperature becomes isotropic on a timescale $(m_e/M_i)^{(1/2)}$ faster than ions. More information on ion acceleration in the absence of electron equilibrium may be found in Refs.[14-15].

The anisotropic nature of the ion motion only takes meaning if the ions are allowed to undergo multiple gyro-orbits before transferring momentum to other species through collisions. This is quantified by the Hall parameter, $\Omega_i > 1$, with

$$\Omega_i \equiv \frac{\omega_{ci}}{\nu_i} \approx 1.5 \times 10^7 \nu_i^{-1} \frac{B}{\mu_i}, \tag{10}$$

where $\nu_i = \nu_{ie} + \nu_{in}$ is the ion collision frequency with both electrons and neutrals. Therefore, thermal anisotropy also requires $\Omega_i > 1$.

The persistence of anisotropy throughout the flow may be characterized by the ratio of the timescale for temperature isotropization, t_{iso}, to the escape time of the plasma through the nozzle time, t_{esc}. We define this ratio as the thermal isotropization parameter, τ_{iso}.

The characteristic escape time may be approximated as the time it takes the plasma to traverse a distance equivalent to its radius at the throat, $r_{p,0}$.

$$t_{esc} = \frac{r_{p,0}}{c_{s,0}} = r_{p,0} \left(\frac{\gamma_e k_b T_{e,0} + 3 k_b T_{\parallel,0}}{M_i} \right)^{-1/2} \tag{11}$$

Here, we have used the fact that the plasma escapes the throat at the ion sounds speed, $c_{s,0}$.[16]

The timescale for temperature isotropization may be obtained from the isotropization rate for the ions,[9]

$$\nu_{iso} \approx 1.9 \times 10^{-14} \frac{\lambda_{ii} n}{\mu_i^{1/2} T_\parallel^{3/2}} \frac{f\left(\Theta_{iso}\right)}{\left(\Theta_{iso}-1\right)^2}, \tag{12}$$

where,

$$f(\Theta_{iso}) = \begin{cases} -3 + \left(\Theta_{iso}+2\right)\left(\Theta_{iso}-1\right)^{-1/2} \tan^{-1}\left(\sqrt{\Theta_{iso}-1}\right) & : \Theta_{iso} > 1 \\ -3 + \left(\Theta_{iso}+2\right)\left(1-\Theta_{iso}\right)^{-1/2} \tanh^{-1}\left(\sqrt{1-\Theta_{iso}}\right) & : \Theta_{iso} < 1 \end{cases}$$

and λ_{ii} is the Coulomb logarithm associated with ion-ion collisions. We may then take the timescale for temperature isotropization as $t_{iso} = \nu_{iso}^{-1}$.

The thermal isotropization parameter for a given magnetic nozzle plasma may be obtained from

$$\tau_{iso} \approx 5 \times 10^{16} \frac{\left(\gamma_e T_{e,0} + 3T_{\parallel,0}\right)^{1/2}}{r_{p,0}} \frac{T_\parallel^{3/2}}{n} \frac{\left(\Theta_{iso}-1\right)^2}{f\left(\Theta_{iso}\right)}, \tag{13}$$

where we have approximated $\lambda_{ii} \approx 10$. It may then be concluded that, if $\Theta_{iso} \neq 1$, $\Omega_i > 1$, and $\tau_{iso} > 1$, the plasma is in a regime where the magnetic mirror force leads to ion acceleration. If any of these requirements are not satisfied, ion acceleration will primarily occur through thermal expansion.

2. Thermal Equilibration

Compared to ions, it is oftentimes easier to heat a confined electron population because very strong magnetic fields are not required. If the equilibration time between ions and electrons is much longer than the confinement time, a plasma is created in which the electrons are thermalized and the ions are cold ($T_e >> T_i$). Some examples are helicon[17–19] and electron cyclotron resonance plasmas.[20] When these plasmas are used with a magnetic nozzle, a balance develops between the thermal expansion of the electrons and the tendency of the plasma to remain quasineutral. An ambipolar electric field results from this balance whose potential drop is nearly that of the electron temperature. Ion acceleration occurs within this potential drop, thus converting electron thermal energy into ion kinetic energy.[21–23]

Allowing for disparate parallel and perpendicular ion temperatures, we define the degree of equilibration between electrons and ions as

$$\Theta_{eq} \equiv \frac{T_e}{T_\parallel/3 + 2T_\perp/3}. \tag{14}$$

Thermal equilibrium between the ions and electrons requires $\Theta_{eq} = 1$.

Similar to ion temperature isotropy, temperature equilibration may be characterized by the ratio of the timescale for thermal equilibration, t_{eq}, to the characteristic escape time, t_{esc}. We will refer to this ratio as the thermal equilibration parameter, τ_{eq}.

The timescale for thermal equilibration between ions and electrons may be obtained from their relative equilibration rate,[9]

$$\nu_{eq}^{e|i} \approx 3.3 \times 10^{-15} \frac{\lambda_{ei} n}{\mu_i T_e^{3/2}}, \tag{15}$$

where λ_{ei} is the Coulomb logarithm for ion-electron collisions.

The thermal equilibration parameter for a given plasma flow is then found from

$$\tau_{eq} \approx 3.0 \times 10^{17} \frac{\left(\gamma_e T_{e,0} + 3T_{\parallel,0}\right)^{1/2}}{r_{p,0}} \frac{\mu_i^{1/2} T_e^{3/2}}{n}. \tag{16}$$

For $\Theta_{eq} > 1$ and $\tau_{eq} > 1$, ion acceleration occurs in a regime where ambipolar effects are dominant. If $\Theta_{eq} < 1$ and $\tau_{eq} > 1$, ions are accelerated through thermal expansion. Finally, if $\tau_{eq} < 1$, ions and electrons equilibrate and ions accelerate through both an ambipolar electric field and ion pressure gradient.

3. Neutral Particles

To this point, we have considered ion acceleration in fully-ionized magnetic nozzle plasmas. It is also possible to have a significant amount of momentum carried by neutral particles within the plasma exhaust due to acceleration through charge-exchange collisions with energetic ions.

Neutral pumping, as defined by Fruchtman,[24] is the process by which charge exchange collisions with ions deplete the neutral population within a plasma source. This is opposed to ion pumping, which is the depletion of neutrals through ionization. For magnetic nozzle applications, neutral pumping results in neutral acceleration and a significant amount of momentum being carried away by a fast neutral population within the exhaust. Using a one-dimensional model, Fruchtman demonstrated that neutral pumping increases the thrust to power of a thermally expanding plasma, but decreases the thrust efficiency. This is because of the drag on the ions and subsequent exit velocity decrease associated with collisions with neutrals.

The first obvious requirement for the significance of neutral particle effects may be expressed in terms of the ionization fraction,

$$\chi_i = \frac{n}{n+N}. \tag{17}$$

The ionization fraction must be less than unity for the neutral particle density, N, to be large enough compared to the plasma density, n.

Assuming the presence of an ample population of neutrals, Fruchtman shows the relative importance of neutral pumping depends on the ratio of the ion-neutral collision frequency, ν_{in}, to the ionization frequency, ν_{ion}. We will denote this ratio as the neutral pumping parameter,

$$\tau_{pump} = \frac{\nu_{in}}{\nu_{ion}} = \frac{t_{ion}}{t_{in}}, \tag{18}$$

which, returning to our timescale notation, represents the ratio of the ionization and charge-exchange collision timescales, t_{ion} and t_{in}, respectively. For $\tau_{pump} > 1$, neutral depletion occurs through neutral pumping. Alternatively, neutral depletion through ion pumping is dominant for $\tau_{pump} < 1$.

The charge-exchange collision timescale can be obtained from the ion-neutral collision frequency,[24]

$$\nu_{in} = 8.99 \times 10^{-16} N T_i^{1/2} \left(\frac{\alpha_R}{\mu_R}\right)^{1/2}, \tag{19}$$

where α_R and μ_R are the relative polarizability and reduced atomic mass (a.m.u), respectively. Furthermore, the ionization timescale may be determined from the ionization frequency,

$$\nu_{ion} = N f_{ion}\left(T_e, \epsilon_i\right). \tag{20}$$

Here, ϵ_i, is the ionization energy of the gas and $f_{ion}\left(T_e, \epsilon_i\right)$ is a function typically determined for a given plasma through empirical means.[25]

The presence of neutrals may lead to a significant drag on the expanding plasma if the timescale associated with charge-exchange collisions is less than the confinement time of the plasma. This phenomenon, which is not explicitly investigated by Fruchtman, may be characterized by the drag parameter

$$\tau_{drag} = \frac{t_{in}}{t_{esc}}. \tag{21}$$

In the equation above, t_{esc} is the escape time defined in Eq.(11). If $\tau_{drag} > 1$, a sizable portion of ions lose momentum to neutrals before exiting the nozzle. However, if $\tau_{drag} < 1$, the ion dynamics are uninfluenced by the neutral population.

4. Current-Free Double Layers

Considerable attention within the plasma propulsion research community has recently been directed towards ion acceleration through current-free double layers (CFDL). First observed in experiments simulating electron acceleration in the aurora, a double layer is a non-neutral discontinuity of the electric potential and plasma density forming between two regions of quasineutral plasma.[26] Charles and Boswell discovered the presence of a CFDL in a helicon plasma expanding through a magnetic nozzle and noted its promise for

propulsion applications.[18] Since this initial discovery, extensive research has gone into the formation, properties, and propulsive performance of CFDL thrusters. It has been suggested by Ahedo,[27] however, that the CFDL is a limiting case of the magnetic nozzle whereby a separate population of hot electrons steepens the aforementioned ambipolar potential. From this analysis, he concludes that ion beam formation in CFDL thrusters still occurs at the expense of electron thermal energy, and predicts no propulsive benefits over magnetic nozzles without CFDLs.

C. Detachment Region

Following acceleration, it is of utmost importance that the plasma beam be able to detach from the guiding magnetic field of the nozzle. If this detachment does not occur with minimal divergence and drag, the application of magnetic nozzles to space propulsion becomes improbable. As such, the physics behind plasma detachment has been a central area of magnetic nozzle research for the past three decades. In this section, we provide a brief review of the results of this research. Furthermore, we present the scaling parameters associated with four detachment mechanisms: three-body recombination, resistive diffusion, demagnetization, and self-magnetization.

1. Plasma Recombination

The detriment caused by eventual closure of the guiding magnetic field may be avoided if a majority of the plasma recombines to form an energetic beam of neutral particles.[28] Free of electric charge, this beam would be impartial to the magnetic topology. Three physical mechanisms exist by which this recombination may occur: three-body collisions with two electrons and an ion, three body collisions with two ions and an electron, and radiative recombination. It has been suggested that the first of these mechanisms is dominant within most laboratory plasmas.[29]

A recombination rate greater than the escape rate of the plasma is the most fundamental requirement for detachment via plasma recombination. Thus, we define the recombination parameter as,

$$\tau_{rec} \equiv \frac{\nu_{esc}}{\nu_{rec}} = \frac{t_{rec}}{t_{esc}}. \tag{22}$$

It may also be shown that

$$\nu_{rec} = n^2 f_{rec}\left(T_e, \epsilon_i, \Delta\epsilon^*\right), \tag{23}$$

where $\Delta\epsilon^*$ is the difference between the ionization energy and the energy of the first excited state and f_{rec} is species dependent and often found empirically.

2. Resistive Diffusion

First proposed by Moses,[30] resistive plasma detachment is the mechanism by which plasma separates from the magnetic nozzle by collisional diffusion across the applied magnetic field lines. However, it was shown by Moses that cross-field diffusion led to a drag force on the plasma, thus decreasing the acceleration efficiency. Additionally, a trade off exists between the desire to decrease losses by minimizing diffusion within the plasma source and the desire to improve the detachment efficiency by increasing diffusion beyond the acceleration region.

Resistive detachment may be characterized by the ratio of the characteristic cross-field diffusion timescale to the confinement time of the plasma. We define this ratio as the diffusion parameter,

$$\tau_{diff} \equiv \frac{t_{diff}}{t_{esc}} = \frac{r_p^2/D_\perp}{r_{p,0}/c_{s,0}} \approx Lu\left(\frac{v_A}{c_s}\right). \tag{24}$$

Above, $D_\perp$ is the cross-field diffusion coefficient, Lu is the Lundquist number, and v_A is the Alfvén speed. For efficiency detachment, it is desirable to evolve from a value of $\tau_\perp >> 1$ in the plasma source to $\tau_\perp \sim 1$ just beyond the acceleration region.

3. Demagnetization

Plasma detachment may occur if the magnetic field decreases to the point where the plasma effectively becomes demagnetized. This may occur either gradually due to the natural decrease of the magnetic field strength as the plasma leaves the nozzle,[2,31] or abruptly as induced currents expel magnetic flux from the bulk of the plasma.[32]

In either the case of gradual or abrupt demagnetization, the ratio of the particle Larmor radius to the scale length of magnetic field variation determines the extent to which the plasma is magnetized. We define this ratio as the magnetization parameter,

$$l_{B,j} \equiv r_{L,j} \left| \frac{\nabla B}{B} \right|, \tag{25}$$

where $r_{L,j}$ is the Larmor radius of species j. As $\hat{l}_{B,j}$ approaches unity, Larmor motion breaks down, and species j effectively becomes demagnetized.

Due to their large mass, the Larmor radius of ions is typically much greater than that of electrons. Eq.(25) then tells us that the ions will demagnetize more readily than electrons. This phenomenon has been observed both experimentally[33] and in numerical simulations.[34]

Electrons, on the other hand, have a Larmor radius that is oftentimes many orders of magnitude smaller than ions. As such, electron motion will remain tied to the magnetic field far downstream the nozzle in the absence of an outside influence. Hooper[31] suggests that ambipolar electric fields effectively couple the electron motion to the inertia of the demagnetized ions. As a result, electron detachment is improved while ion detachment is hindered, and the plasma as a whole detaches according to Eq.(25) as if it were a species of hybrid particles of mass $m_H = (m_e M_i)^{1/2}$.

Two-fluid simulations by Ahedo and Merino,[34] however, suggest that the assumption of local ambipolarity, central to Hooper's thesis, breaks down when two-dimensional effects are included. In this case, the ambipolar electric field does not have to be on the same order as the ion inertia, and electrons remain tied to the magnetic field. As such, plasma detachment only occurs in the limit of electron demagnetization.

As we recall from section 2, a plasma may become demagnetized as β_p approaches unity due to its diamagnetic nature. Independent simulations by Lorzel and Mikelledes,[35] and Sankaran and Polzin,[36] each show the expansion of a high-β plasma whose diamagnetic currents effectively shield the applied flux from the body of the plasma throughout the entirety of the nozzle. The result is the expansion of an unmagnetized plasma confined within a magnetized resistive layer.

Recent simulations[32] by Merino and Ahedo show that diamagnetic currents may lead to the expulsion of magnetic flux from the plasma downstream from the nozzle throat. As flux is expelled, a seperatrix forms which is defined by the surface of zero magnetic field. This seperatrix was observed to move closer to the nozzle throat as the value of β_p at the throat increased. Because β_p increases downstream from the throat, it is reasonable to suspect that the seperatrix forms as the local value of β_p approaches unity. In this case, confinement breaks down and abrupt demagnetization of the plasma likely occurs. Experiments on a Helicon source expanding through a magnetic nozzle confirm the existence of this seperatrix.[37] Further investigation of the plasma dynamics near the seperatrix is required before the performance implications of this detachment mechanism can be fully understood.

4. Magnetic Detachment

The influence of induced magnetic fields that augment, as opposed to expel, the applied magnetic field has also been proposed as a detachment mechanism for magnetized plasma flows. Using MHD theory,[38,39] Arefiev and Breizman showed that the magnetic fields of the nozzle may become stretched along with the flow by an azimuthal current density that develops within the plasma. The propensity of the flow to stretch the magnetic field depends on the parameter

$$\beta_k \equiv \frac{m_i n u^2}{B^2/\mu_0}, \tag{26}$$

which represents the ratio of the kinetic energy of the flow to the magnetic field energy. We will refer to β_k as the kinetic-beta, and β_p as the plasma-beta. Arefiev and Breizman claim that, as β_k approaches unity, the plasma will drag the field along with the flow, effectively detaching itself from the nozzle. However, the physical source of the induced currents was unclear from their analysis.

Using a two-fluid model, we showed in a previous paper that the induced currents that develop within the plasma are the result of deviations of the particles from their initial flux surface.[40] Through the conservation of canonical angular momentum, an azimuthal current density arises. It is this current density that tends to drag the magnetic field along with the flow. It was ultimately observed that the stretching of the magnetic field only occurred so long as the plasma remained magnetized.

III. Quasi-One-Dimensional Theory

The expansion of a magnetic nozzle plasma encompass densities and magnetic fields that progress through many orders of magnitude. As a result, the dimensionless parameters characterizing the behavior of the plasma will evolve throughout the expanding plume. As such, the goal of this section is to use a quasi-one-dimensional model for the expansion of an anisotropic, non-equilibrium magnetic nozzle plasma to determine how the nature of the plasma changes in the downstream portion of a magnetic nozzle.

A. Fundamental Equations

Quasi-one-dimensional models for the expansion of a magnetic nozzle plasma are relatively common in the literature. Andersen[1] considered the ions and electrons as an isothermal fluid to solve for the Mach number and density variations of the flow with changing flux tube area. Chubb[41] provided a similar analysis, but also included a consisted description for the ion and electron energy equations. Saka[16] investigated the influence of ion temperature anisotropies on the sonic condition. Furthermore, Ahedo and Merino[34] compared a model similar to Andersen's to their two dimensional results and found good agreement for the axial evolution of many of the plasma parameters. Finally, Fruchtman[24] investigated the influence of charge-exchange collisions and ionization on a constant area plasma flow.

Thus far, none of the previous one-dimensional models have investigated the influence of both ion temperature anisotropies or electron-ion non-equilibrium. To this end, we develop the equations for the expansion of a fully ionized, collisionless, quasi-neutral plasma that allows both ion temperature anisotropy ($T_\parallel \neq T_\perp$) and disparate electron and ion temperatures ($T_e \neq T_i$). We assume the electron temperature remains isotropic as the isotropization timescale for electrons is of order $(m_e/M_i)^{1/2}$ smaller than that of ions.

Combining the continuity equation of either species with the law $\nabla \cdot \mathbf{B} = 0$, we arrive at

$$\frac{d}{dz}\left(\frac{nv}{B}\right) = 0, \tag{27}$$

where n is the plasma density, v is the plasma velocity, and B is the magnitude of the magnetic field. z represents the axial distance along the nozzle axis, with $z = 0$ defining the location of the nozzle throat.

We ignore electron inertia and collisions, from which the electron and ion momentum equation yield

$$0 = en\frac{d\phi}{dz} - \frac{dp_e}{dz}, \tag{28}$$

and

$$nM_i v\frac{dv}{dz} = -en\frac{d\phi}{dz} - \frac{dp_\parallel}{dz} + \frac{\left(p_\parallel - p_\perp\right)}{B}\frac{dB}{dz}, \tag{29}$$

respectively. The pressure is given by the ideal gas law, $p = nk_bT$, where k_b is Boltzmann's constant.

In Eq.(29), we see the three mechanisms by which ion acceleration occurs: (1) the transfer of electron thermal energy, p_e, by means of the ambipolar potential, ϕ; (2) pure thermal expansion along the magnetic field lines, as shown in the second term on the right hand side; and (3) conservation of the first adiabatic invariant, or the magnetic mirror force, as seen in the last term. Also, we note that the magnetic mirror force disappears for isotropic ion temperatures.[13]

Eq.(27)-(29) need to be closed with energy equations for the ion perpendicular, parallel, and electron temperatures. We assume for now that the electron flow is isentropic and that the ion temperatures follow the double-adiabatic laws. We then obtain the closure relations,

$$\frac{d}{dz}\left(\frac{T_e}{n^{\gamma-1}}\right) = 0, \tag{30}$$

$$\frac{d}{dz}\left(\frac{T_\perp}{B}\right) = 0, \tag{31}$$

$$\frac{d}{dz}\left(\frac{T_{\parallel}B^2}{n^2}\right)=0, \tag{32}$$

where γ_e is the electron specific heat ratio. As we will see later, the evolution of the plasma similarity parameters depends strongly on the electron temperature, which in turn depends strongly on γ_e.

Assuming the plasma is of low enough β_p such that induced magnetic fields are negligible, Eqs.(27-32) represent six equations for the six unknowns: n, ϕ, v, T_e, $T_{\parallel}$ and $T_{\perp}$.

B. Numerical Solution

Before solving the quasi-one-dimensional model, we non-dimensionalize the magnetic field, density and temperatures by their values at the throat of the nozzle. These dimensionless parameters are denoted with the hat-notation. The axial distance is normalized by the radius of the coil, $\hat{z}=z/r_c$, and the dimensionless velocity is given by $\hat{v}=v/c_{s,0}$ where $c_{s,0}$ is the parallel ion sounds speed as defined in Eq.(11).

Inserting Eq.(28) into Eq.(29), and simplifying using Eq.(27) and Eqs.(30-32) yields a differential equation for the evolution of the plasma velocity along the length of the nozzle for a given magnetic field:

$$\left[1-\frac{\hat{f}_e}{\hat{v}^2}\left(\frac{\hat{B}}{\hat{v}}\right)^{\gamma_e-1}-\frac{\hat{f}_{\parallel}}{\hat{v}^4}\right]\hat{v}\frac{d\hat{v}}{d\hat{z}}=-\left[\frac{\hat{f}_e}{\hat{B}}\left(\frac{\hat{B}}{\hat{v}}\right)^{\gamma_e-1}+\hat{f}_{\perp}\right]\frac{d\hat{B}}{d\hat{z}}, \tag{33}$$

where,

$$\hat{f}_e=\frac{\Theta_{eq,0}\left(2\Theta_{iso,0}+1\right)}{\Theta_{eq,0}\left(2\Theta_{iso,0}+1\right)+9/\gamma_e}, \tag{34}$$

$$\hat{f}_{\parallel}=\frac{9/\gamma_e}{\Theta_{eq,0}\left(2\Theta_{iso,0}+1\right)+9/\gamma_e}, \tag{35}$$

$$\hat{f}_{\perp}=\frac{9\Theta_{iso,0}/\gamma_e}{\Theta_{eq,0}\left(2\Theta_{iso,0}+1\right)+9/\gamma_e}, \tag{36}$$

result from the normalization and are functions of the ion temperature anisotropy and species non-equilibrium at the nozzle throat, $\Theta_{iso,0}$ and $\Theta_{eq,0}$, respectively. Furthermore, we note the requirement that $\hat{v}=1$ at the nozzle throat for continual acceleration, thus fulfilling the sonic condition.

Eq.(33) may be integrated numerically, after which the axial dependence of the plasma density and temperatures may be obtained from the modified continuity equation and three closure relations:

$$\hat{n}=\frac{\hat{B}}{\hat{v}},\quad \hat{T}_e=\hat{n}^{\gamma_e-1},\quad \hat{T}_{\parallel}=\frac{\hat{n}^2}{\hat{B}^2},\quad \hat{T}_{\perp}=\hat{B}. \tag{37}$$

The inputs to the model are the magnetic field profile, $\hat{B}\left(\hat{z}\right)$, electron specific heat ratio, γ_e, initial isotropy, $\Theta_{iso,0}$, and initial species non-equilibrium, $\Theta_{eq,0}$. Using these inputs, the magnitude of Eqs.(34-36) determine the relevant ion acceleration mechanism.

For the results presented here and the next section, the magnetic field profile is assumed to fall off as a magnetic dipole, or $\hat{B}=\left(1+\hat{z}\right)^{-3/2}$. Furthermore, four different solutions will be presented that investigate the influence of: (1) varying the electron specific heat ratio for a cold ion plasma ($T_{\parallel}=T_{\perp}=0$), and (2) varying the ion temperature isotropy for a cold electron plasma ($T_e=0$).

The first two solutions represent the expansion of a hot-electron plasma source for two values of the electron specific heat ratio: isothermal electrons, $\gamma_e=1.0$, and isentropic electrons, $\gamma_e=5/3$. For these solutions, ee set $\Theta_{eq,0}=10^5$ so that ion thermal effects may be ignored, and arbitrarily let $\Theta_{eq,0}=1$, although it has no influence on the result.

The resulting axial density, Mach number, and electron temperature profiles for the first two solutions may be seen in Fig.1(a)-1(c). We adopt the notation: $[X]=\log_{10}\left(X\right)$. The red solid lines represent isothermal electrons, while the blue solid lines represents $\gamma_e=5/3$. First, it is observed that the isothermal electron density falls off fastest, from which Eq.(37) indicates that ion acceleration occurs more quickly for isothermal electrons. Second, the Mach number for isothermal electrons increases more slowly than for $\gamma_e=5/3$, as would be expected from the fact that $M\sim T_e^{-1/2}$.

The last two solutions that we present look at the effect of varying the initial ion temperature anisotropy. We consider $\Theta_{iso,0}=10$, and $\Theta_{iso,0}=100$ for a cold electron plasma, or $\Theta_{eq,0}=0$. The results of these

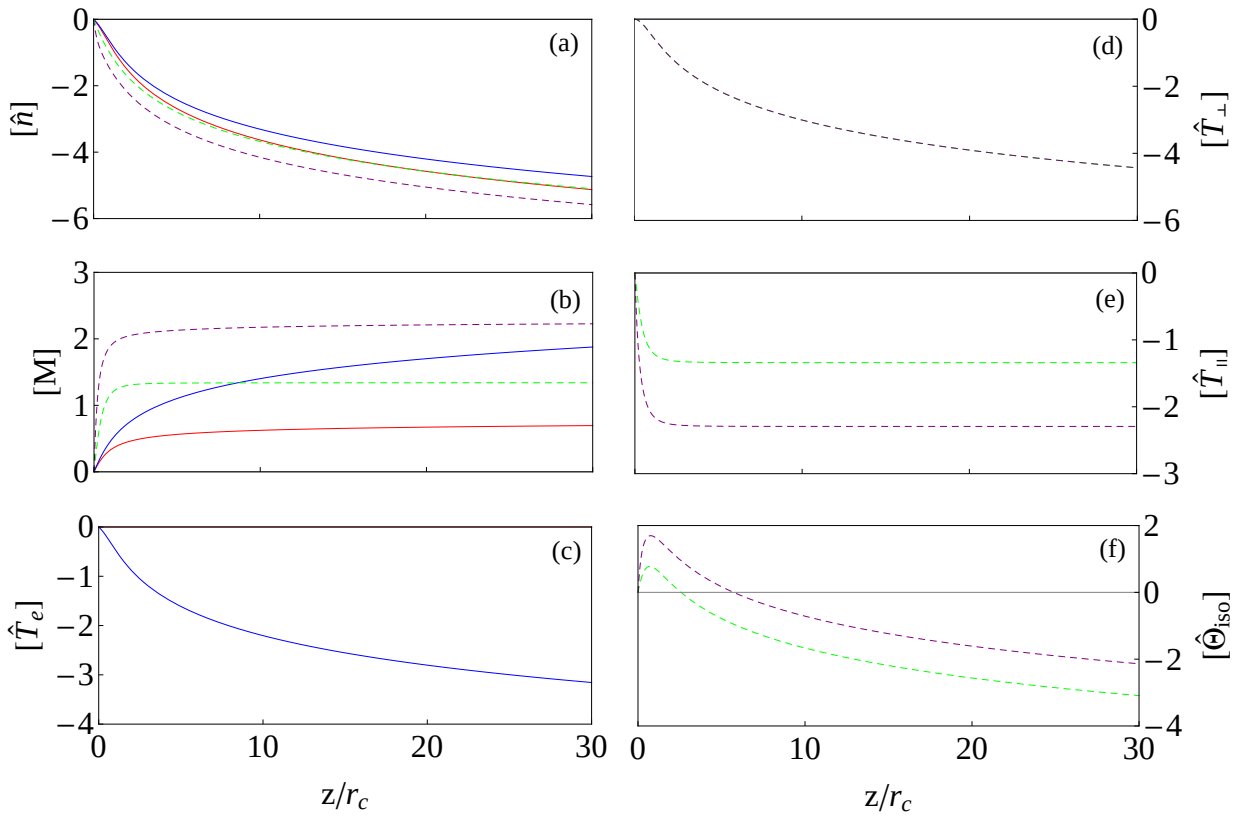

Figure 1. Axial variation of: (a) plasma density, (b) Mach number, (c) electron temperature, (d) ion perpendicular temperature, (e) ion parallel temperature, and (f) ion anisotropy. Each parameter is presented in the form: $[\hat{X}] = \log_{10}(X/X_0)$, where X_0 is the value at the throat ($z = 0$). Lines represent solutions with the following properties: isothermal electrons (solid red) $\gamma_e = 1$, $\Theta_{eq,0} = 10^5$, $\Theta_{iso,0} = 1$; isentropic electrons (solid blue) $\gamma_e = 5/3$, $\Theta_{eq,0} = 10^{-4}$, $\Theta_{iso,0} = 1$; cold electrons, anisotropic ions (dashed green) $\gamma_e = 1.2$, $\Theta_{eq,0} = 0$, $\Theta_{iso,0} = 10$; cold electrons, anisotropic ions (dashed purple) $\gamma_e = 1.2$, $\Theta_{eq,0} = 0$, $\Theta_{iso,0} = 100$

solutions are presented in Fig.(1), where the dashed green line corresponds to $\Theta_{iso,0} = 10$ and the dashed purple line $\Theta_{iso,0} = 100$.

It may be seen that ion acceleration through the magnetic mirror force pushes the acceleration region closer to the nozzle throat as compared to ion acceleration through ambipolar electric fields. Furthermore, the larger the anisotropy, the more quickly the ions accelerate. Fig.1(d) indicates that the axial variation of the normalized perpendicular ion temperature is irrespective of the initial anisotropy; a fact that is supported by the conservation of the first adiabatic invariant, or Eq.(31). It is also seen that the normalized parallel ion temperature eventually reaches an asymptotic value, which decreases with increasing anisotropy. Finally, the local value of the normalized anisotropy, $\hat{\Theta}_{iso} = \Theta_{iso}/\Theta_{iso,0}$, increases just beyond the nozzle throat but eventually decreases as the parallel ion temperature asymptotes.

In the four cases presented above, we immediately realize the large variation between the different solutions of the axial profile of the plasma Mach number, electron temperature, parallel velocity, and anisotropy of the plasma. As we will show in the next section, these differences become critical when considering the evolution of the similarity parameters of the plasma.

IV. Magnetic Nozzle Expansion

Understanding the scaling of the different plasma acceleration and detachment mechanisms from a magnetic nozzle is the focus of this section. We begin by reviewing the main discoveries of previous magnetic nozzle laboratory experiments and compile a table of their plasma properties prior to expansion. Using the values from this table, we compute the similarity parameters for each experiment. Finally, we use the results

of the one-dimensional model presented in the previous section to determine the evolution of the similarity parameters to determine the relevant physical phenomenon governing plasma expansion.

A. Magnetic Nozzle Laboratory Experiments

We begin with a brief description of each of the ten laboratory experiments included in this analysis. The experiments were chosen to be representative of the wide array of operational parameters associated with magnetic nozzles. These parameters may be seen in Table 1. The main findings of each experiment are summarized below:

1. Andersen:[1] This paper, published in 1969, is the first experimental study demonstrating that a magnetic nozzle acceleration is physically possible. The magnetic Laval nozzle in this experiment is obtained by modifying the uniform axial magnetic field configuration of a Q device with a region of high magnetic field ($\sim 10kG$). A cesium gas is used to produce continuous supersonic plasma flows with Mach numbers of approximately 3. This formed the basis for further investigation into employing the nozzle for producing supersonic plasma jets for propulsion and other applications.

2. Kuriki and Okada:[21] Kuriki demonstrates experimentally the electrostatic ambipolar acceleration of ions in the downstream region of a magnetic nozzle. Plasma is formed from an arcjet and subsequently expanded through the magnetic field of a concentric current loop. The data shows that the maximum velocity of the ions at the end of the nozzle greatly exceeded expectations from isentropic expansion, which suggests that the ions are accelerated from ambipolar electric fields. The plasma is shown to follow the magnetic field lines, thus giving no evidence of detachment.

3. York at al.:[42] A θ-pinch device is used to create a high-β plasma prior to expansion through a magnetic nozzle. York ultimately finds that the behavior of the plasma through the magnetic nozzle is governed mainly by electromagnetic effects as opposed to pure isentropic expansion. This is likely due to the large plasma β, as significant perturbations to the applied field take place. Electron thermal conduction is observed to be an order of magnitude larger than classical values predict.

4. Deline et al.:[43] By examining the expansion of a magnetized pulsed washer gun plasma,[44] Deline finds that plasma separation from the applied magnetic field occurs as β_k approaches unity, where β_k is defined as in Eq.(26). This is the first experiment specifically designed to observe and characterize plasma detachment.

5. HYPER-I:[33] Terasaka maps the ion streamlines of an ECR plasma flowing through diverging magnetic fields. He also notes the importance of the ambipolar electric field on ion acceleration. He observes that detachment of the ions from the applied magnetic field occurs at a point where ion magnetization breaks down, suggesting that the plasma detaches according to demagnetization. The effect of electrons is not included in his study.

6. L-PMPI:[45] Detachment of the plasma from the applied magnetic field is demonstrated for an inductively coupled plasma (ICP) expanding through an applied magnetic field generated with permanent magnets. Acceleration through a double layer is claimed, however, the length over which the potential drop occurs is much greater than that of a typical double layer. The specific detachment mechanism is not investigated in detail.

7. HDLT:[19] West characterizes the expansion the Helicon Double Layer Thruster (HDHT): a low density, low magnetic field helicon plasma in the presence of a double-layer. He concludes that ion detachment must occur because the ion gyrodius becomes greater than the scale of the experiment downstream from the plasma source.

8. HPHT:[5,37] The High-Power-Helicon Thruster (HPHT) is used to investigate the influence of a high-density, low magnetic field (high-β) plasma source on the magnetic field topology of a magnetic nozzle.[5] It is ultimately found that the plasma diamagnetism expels magnetic flux from the body of the plasma and results in a seperatrix at which the magnetic field disappears.[37] The implications of this seperatrix on detachment were not investigated in detail.

ID	Name/Author	Source	Gas	$n(m^{-3})$	$T_e(eV)$	$T_i(eV)$	$B_0(T)$	$r_{p,0}(m)$	χ_i
1	Andersen[1]	Q-Machine	Cs	10^{18}	1	[0.1][46]	1	0.01	0.99
2	Kuriki[21]	Arcjet	Ar	10^{19}	0.5	0.1	0.1	0.01	10^{-4}
3	York[42]	θ-pinch	D	10^{22}	30	{30}	2.3	0.038	0.7
4	Deline et al.[43]	Washer Gun	H	10^{19}	1	[0.1][44]	0.07	0.02	0.5
5	HYPER-I[33]	ECR	Ar	10^{17}	7.5	[0.1][20]	0.12	0.15	0.1
6	L-PMPI[45]	RF-ICP	Ar	10^{17}	8	[0.1][47]	0.02	0.033	10^{-3}
7	HDLT[19]	Helicon	Ar	10^{17}	6.3	[0.1][48]	0.0138	0.07	0.003
8	HPHT[5,37]	Helicon	Ar	10^{19}	10	[0.1][48]	0.03	0.035	0.5
9	MNX[22]	Helicon	Ar	10^{19}	7	0.5	0.14	0.02	0.9
10	VASIMR[7,10,23]	Hel.+ICRH	Ar	[10^{20}][23]	[10][23]	[40][10]	[2][7]	{0.1}	[0.99][7]

[ ][a]-values obtained from Ref[a]. { }-value is an estimation

Table 1. Plasma parameters for ten different magnetic nozzle experiments. The numbers for experiments 1-9 represent real quantities, while the numbers for VASIMR are a combination of measured and expected values.

9. MNX:[22] Ion acceleration in the Magnetic Nozzle Experiment (MNX) is observed for a high density, high magnetic field plasma. Supersonic ion beams are observed, from which it is concluded that ion acceleration occurs through ambipolar electric fields rather than ion pressure effects or magnetic moment conservation.

10. VASIMR:[7] VASIMR is an electric propulsion concept based on expanding a helicon generated, ICHF heated plasma through a strong permanent magnet nozzle. Through this two-stage plasma generation-heating process, they are able to achieve high densities and temperatures. The values provided in Table 1 are estimates based on present studies and predicted performance.

For each experiment, the plasma parameters presented in Table 1. may be found in the reference included in the experiment name/author column, unless otherwise noted. Furthermore, each value represents the measurement of the parameter at the nozzle throat.

B. Expansion Physics

The plasma similarity parameters of the previously described experiments will be presented here along with their evolution throughout the exhaust plume as determined from the simplified one-dimensional model from Section III. It should be noted that the solutions to the one-dimensional model are for a collisionless plasma, while many of the similarity parameters are based on collisionality. With that said, the main goal of the one-dimensional model is to characterize collisionless expansion and determine the conditions under which the collisionless assumption breaks down.

We divide the similarity parameters into the following categories that describe their relevance: plasma quality, magnetic confinement, acceleration and detachment. Each category contains figures that compare the values of two related dimensionless quantities for all of the experiments in Table 1. Furthermore, the evolution of these parameters with respect to their initial value is presented for the four solutions given in Section III. Again, we adopt the convention, $[\hat{X}] = \log_{10}(\hat{X})$, where the hat notation indicates normalization of X with respect to its initial value.

We note that, with the exception of the York experiment and VASIMR, the expansion of all of the experiments is driven mainly by electron thermal energy because their electron temperatures are greater than their ion temperatures. As such, the evolution of their similarity parameters is most appropriately described by the solid line solutions, which depict $\gamma_e = 1$ (red) and $\gamma_e = 5/3$ (blue).

1. Plasma Quality

Recalling from Section II.A.1., one of the most fundamental requirements of a plasma is its ability to shield charge. This was expressed in terms of requirements on the normalized Debye length and plasma parameter,

$l_D << 1$ and $\Lambda_P >> 1$, respectively. The values of these two parameters for the experiments in Table 1 are shown in Figure 2(a).

It is clear from Figure 2(a) that all of the laboratory magnetic nozzle plasmas meet the plasma requirements for the Debye length and plasma parameter. Furthermore, the evolution of these parameters, shown in Figures 2(b) and 2(c), indicates that the plasma requirement will hold throughout the plume. As Merino and Ahedo have shown,[32] breakdown of the Debye length requirement may be possible at the rarefied plasma edge. However, this is a two-dimensional effect and, as such, cannot be included in this analysis.

The applicability of the fluid description of each species within a plasma may be ascertained from their respective Knudsen numbers, where the Knudsen number is defined as the ratio of the collisional mean free path to the scale length of the plasma. If the Knudsen number is much less than unity, collisions will be frequent enough to randomize the species motion and relax the particles toward a Gaussian velocity distribution function. As such, the dynamics of that species is well approximated by the fluid equations.

The ion and electron Knudsen numbers for each experiment may be seen in Figure 3(a). We see that the low ionization fraction of the Arcjet (Exp. 2) leads to small mean free paths through neutral collisions, and subsequently small Knudsen numbers. If neutral collisions are neglected, the Knudsen number of each species scales as $Kn_j \propto T_j^2/n$, thus the higher density experiments such as the θ-pinch plasma and VASIMR both have Knudsen numbers less than unity. However, The low temperatures of the Q-machine and washer gun plasmas lead to larger Knudsen numbers. Finally, with the exception of VASIMR, both the ion and electron Knudsen numbers for the wave generated plasmas (Exp. 5-9) are near or greater than unity. This indicates that, while still useful from a conceptual standpoint, fluid models are not appropriate to describe these plasmas at the nozzle throat.

Figures 3(b) and 3(c) show that, unless sufficient electron cooling occurs ($\gamma_e = 5/3$), the Knudsen number of each species will increase by many orders of magnitude downstream the throat. In the absence of a cooling mechanism, a complete description of plasma expansion downstream the magnetic nozzle throat for all highly ionized plasmas likely requires a kinetic formulation. Electron temperature measurements in the downstream region of many different plasma sources have produced varying results,[21,42,43] thus understanding electron energy transport in magnetic nozzles becomes critical.

2. Confinement

Proper confinement of the plasma sets requirements on the normalized Larmor radii of the electrons (l_e) and ions (l_i), while the influence of the plasma on the magnetic field of the nozzle is characterized by the ratio of the thermal energy of the plasma to magnetic field energy, β_p, and magnetic Reynolds number, Re_M.

The Larmor radii of ions and electrons normalized by the plasma radius at the throat for each experiment is presented in Figure 4(a). Immediately we see that the normalized ion Larmor radius is greater than the electron Larmor radius in each case. This difference is mainly due to the large ion mass. As expected, we see that the experiments with the largest magnetic fields ($\sim 1T$) have smaller Larmor radii ($l_i \sim 10^{-2}$ and $l_e \sim 10^{-4}$), while weaker magnetic fields ($\sim 0.01T$) lead to relatively large Larmor radii ($l_i > 10^{-1}$ and $l_e \sim 10^{-2}$).

The axial evolution of the electron and ion Larmor radii according to the one-dimensional model may be seen in Figs. 4(b) and 4(c), respectively. The normalized ion Larmor radius is seen to remain constant throughout the plume. This is due to Eq.(31) which dictates that $T_\perp \sim B$. Because $l_i \sim (r_p B)^{-1} T_\perp^{1/2}$ and, through flux conservation, $r_p \sim B^{-1/2}$, we ultimately find that the ratio of the ion Larmor radius to the plasma radius remains constant while the magnetic moment is conserved.

The normalized electron Larmor radius, on the other hand, is seen to increase through many orders of magnitude if the electrons are assumed isothermal (Fig. 4(c)). However, if the electron temperature decreases downstream from the throat, the increase occurs at a much slower rate. Once again, we note the importance of the electron temperature evolution in the nozzle plume, as it will dictate whether or not the electron Larmor radius for low magnetic field nozzles becomes on the order of the plasma radius within a reasonable distance from the nozzle throat.

The influence of the plasma on the confining magnetic fields is characterized by β_p and the magnetic Reynolds number, Re_M. Comparisons of these two values for each experiment may be seen in Figure 5(a). Depending mainly on the magnetic field strength and plasma density, the value of β_p varies widely between $\sim 10^{-6}$ and $\sim 10^{-1}$. The high-β_p plasmas, characteristic of either very large densities (Exp. 3) or low magnetic fields (Exp. 8), would indicate significant perturbations to the applied magnetic field. These

perturbations, brought about by diamagnetic currents induced by the plasma pressure, were observed in the HPHT.[37]

A large variation among the experimental values for the magnetic Reynolds number is also observed. For these values, we used the sound speed at the nozzle throat as the characteristic velocity, the plasma radius as the characteristic length, and the Spitzer value for the resistivity of a fully-ionized plasma. The later may cause significant error in the values for experiments 2 and 6 due to their low ionization fractions. It is seen that, with the exception of the low electron temperature plasmas ($T_e \sim 1eV$), the Magnetic Reynolds number is greater than unity in most cases, and diffusion of the magnetic field into the plasma near the throat of the nozzle may be ignored.

The axial evolution of β_p and Re_M are shown in Figs. 5(b) and 5(c), respectively. If the electrons are isothermal, β_p decreases immediately downstream from the throat, followed by an increase through many orders of magnitude. Furthermore, Re_M increases by many orders of magnitude in the downstream plasma. If the electrons are allowed to cool, however, the increase in β_p occurs much more slowly, and Re_M decreases through many orders of magnitude. If the ions are the primary carrier of thermal energy, the initial decrease in β_p occurs through a larger distance from the nozzle, and the eventual increase is much slower, while Re_M increases at a rate slower than that of isothermal electron expansion.

3. Acceleration

We recall from section II.B. that the ion acceleration mechanism, in the absence of double layers, mainly depends on the ion temperature isotropy and ion-electron thermal equilibrium. Furthermore, the amount of momentum carried by neutrals in the exhaust depends on neutral pumping and neutral drag.

Ion acceleration through magnetic moment conservation, or the magnetic mirror force, required both the ion Hall parameter, Ω_i, and the ratio of the ion temperature isotropization timescale to the escape time, τ_{iso}, be much larger than unity. We will examine these requirements for the θ-pinch plasma and VASIMR as they are the only two experiments with $T_i \geq T_e$. Figure 6(a) shows that the ion hall parameter for these two experiments is greater than unity, and that it increases slightly in the acceleration region immediately downstream the throat. The isotropization parameter, however, is greater than unity for VASIMR and less than unity for the θ-pinch, and decreases in the acceleration region. Here, we have used the value $\Theta_{iso,0} = 10$ for VASIMR and $\Theta_{iso,0} = 1$ for the θ-pinch. It may then be said that ion acceleration occurs due to magnetic moment conservation for a plasma with parameters similar to those predicted in Table 1 for VASIMR. If the plasma density is increased such as in the θ-pinch, collisionality will ensure the isotropization of ion temperatures, and ion acceleration will occur primarily due to ion thermal expansion.

If the electron temperature is greater than the ion temperature, as it is in the remaining experiments, ions will be accelerated through an ambipolar electric field that manifests from the thermal expansion of the electrons. The case may arise, however, where the ions and electrons reach thermal equilibrium prior to expansion, whereby the ions are accel

Neutral particles may influence the acceleration process through charge exchange collisions with ions. If a significant fraction of the neutral population gets swept away in the plume as opposed to ionized, neutral pumping is said to occur.[24] This process is characterized by the neutral pumping parameter, τ_{pump}, whereby a value of $\tau_{pump} > 1$ indicates the timescale for neutral depletion through ionization is greater than that of charge exchange processes.

Figure 8(a) shows that the neutral pumping parameter is only greater than one for the arcjet and washer gun experiments. For these values, we have used Lotz's empirical model for collisional ionization.[25] The large pumping parameters are due to the very low temperatures in the argon arcjet plasma and the low temperature, low mass, and high ionization potential of the washer gun hydrogen plasma. Therefore, except for these two experiments, neutral depletion is expected to occur through ionization. Figure 8(c) suggest that, if the electron temperature decreases rapidly downstream, ionization becomes negligible and neutral pumping dominates.

The ability of neutrals to steal momentum away from the ion population is characterized by the drag parameter, τ_{drag}. This parameter represents the ratio of the charge exchange timescale to the confinement time of the plasma. If $\tau_{drag} > 1$, the majority of the ions are unaware as to the presence of neutrals. Figures 8(a) and 8(c) indicate that neutral drag is only important in plasmas of very high density, or very low ionization, and becomes less important in the downstream, rarefied plasma.

4. Detachment

It has been theorized that plasma detachment may occur by means of plasma recombination, resistive diffusion, demagnetization, and induced magnetic fields. A brief review of these detachment mechanisms was given in Section II.C.4. We should note that, because collisionality in the expanding plasma is so low, a fluid model may not be able to capture all of the physics of a plasma that detaches downstream from the nozzle throat. As such, the assumptions behind the one-dimensional model in Section III are no longer met. With that said, the results obtained for the evolution of the similarity parameters should still be accurate to within a few orders of magnitude.

The dimensionless parameters associated with detachment via three-body recombination and classical resistive diffusion may be seen in Figure 9(a). τ_{rec} is the ratio of the recombination timescale to the confinement time. As such, a value of $\tau_{rec} < 1$ is required for the significance of recombination detachment. However, as Figs. 9(a) and 9(c) show, this detachment process is only likely for very high density, low-temperature plasmas whose electron temperature decreases downstream. This result was previously shown by Dimov.[29]

It may also be seen that the timescale for classical cross-field diffusion is greater than the confinement time, or $\tau_{diff} > 1$, for all of the plasmas in consideration. Similar to recombination detachment, classical resistive diffusion only becomes viable for high density plasmas whose electron temperature drastically decreases during expansion: a fact initial mentioned by Hooper.[31] It should be noted that Spitzer's resistivity for a fully ionized gas was used to determine the values for τ_{diff} in Fig. 9(a), thus the results for Exps. 2 and 7 invalid. Furthermore, enhanced diffusion through turbulent instabilities may decrease the value of τ_{diff} significantly. However, the relation between non-classical cross-field diffusion and plasma detachment has not been investigated in detail.

Detachment through gradual demagnetization, or inertial detachment, is characterized in Figs. 10(a) and 10(c). According to Hooper,[31] separation of the plasma flow from the applied magnetic field scales with the hybrid Larmor radius, l_H. Recently, we showed that this separation occurs as the magnetization parameter, defined as the ratio of the local value of the hybrid Larmor radius to the scale length of magnetic variation, approaches unity.[2] At this point, under Hooper's set of assumptions, the plasma is effectively demagnetized.

Fig. 10(c) plots the axial evolution of the magnetization parameter normalized by l_H at the nozzle throat, $\hat{l}_B = l_B/l_{H,0}$, where l_B is defined in Eq.(25). According to Fig. 10(c), gradual demagnetization of the plasma will occur in the downstream region at a location that depends on the cooling rate of the electrons. However, plasmas that are highly magnetized (small l_H) will not detach until very far downstream ($z/r_c > 30$), and may follow the turning magnetic field lines back towards the nozzle.

One such mechanism to avoid the problem of flow reversal is the abrupt demagnetization of the plasma by induced diamagnetic currents.[32] This likely occurs near the axial location where $\beta_p \approx 1$. According to Figs. 5(a) and 5(b), for an initial $\beta_p > 10^{-4}$, the position of abrupt demagnetization would occur within tens of nozzle radii from the throat for isothermal electrons. If significant electron cooling occurs, however, this process would only be important in the near downstream region for plasmas with $\beta_p \sim 10^{-1}$. Furthermore, the dashed lines indicate that this detachment mechanism seems unlikely if the expansion is governed by ion thermal energy.

Finally, Arefiev and Breizman suggest that paramagnetic currents may be induced within the plasma that stretch the magnetic field along with the flow as β_k approaches unity. Here, β_k is defined in Eq.(26), and represents the ratio between the kinetic energy of the flowing plasma and the energy stored within the magnetic fields.

The value of β_k at the nozzle throat for each experiment is shown in Fig. 10(a), while Fig. 10(b) shows the evolution of this parameter through the downstream region. It is observed that the evolution of β_k is independent of the input parameters to the one-dimensional model. Similar to β_p, plasmas with an initial value of $\beta_k > 10^{-4}$ will have their local β_k approach unity within an axial distance of tens of nozzle radii. If this is the case, the thermal energy and kinetic energy of the plasma may both exceed the magnetic energy near the same axial location, and detachment via abrupt demagnetization may then be at odds against detachment through induced magnetic fields. The relationship between these two detachment mechanisms has not been investigated in detail.

V. Conclusions

The wide variety of magnetic nozzle plasmas has motivated a concise review of the dimensionless parameters describing the relevant plasma physics for the source, acceleration, and detachment regions of a magnetic nozzle. Similarity parameters representing the plasma quality and confinement within the source region were considered. The stability of the plasma source was left for future studies. In the acceleration region, the effects of ion temperature anisotropy, species non-equilibrium, and neutral particles was characterized. However, the influence of double layers on ion acceleration was omitted. Finally, parameters governing plasma detachment via three-body recombination, resistive diffusion, demagnetization, and induced magnetic fields were reviewed.

The expansion of a magnetic nozzle plasma encompasses many different time and length scales. As such, a quasi-one-dimensional fluid model was developed to allow for ion acceleration through magnetic momentum conservation and ion and electron thermal expansion. Using this model, we solve for the axial variation of the ion velocity, plasma density, electron temperature, and perpendicular and parallel ion temperatures for four different cases: hot isothermal electrons with cold ions; hot isentropic electrons with cold ions; cold electrons with an ion anisotropy, $\Theta_{iso} = 10$; and cold electrons with an ion anisotropy, $\Theta_{iso} = 100$.

Ten laboratory experiments were introduced that represent the large array of operational parameters for magnetic nozzle plasmas. These plasmas were characterized using the similarity parameters reviewed in Section II. Furthermore, the evolution of these similarity parameters downstream the nozzle throat was solved for using the quasi-one-dimensional fluid model.

Multiple conclusions are supported in regards to the laboratory plasmas in consideration:

- The evolution of the electron temperature has a profound influence on the nature of the plasma downstream from the nozzle throat.
- In the absence of an electron cooling mechanism, kinetic models are likely required to capture all of the physics related to plasma detachment. They are also more appropriate than fluid models to describe the acceleration region of most RF generated plasmas.
- Magnetic moment conservation only plays a role in ion acceleration for plasmas with significant ion anisotropies, moderate densities ($n \sim 10^{20} m^{-3}$) and large confining magnetic fields ($B \sim 1T$).
- The timescale for equilibration between electron and ion temperatures is much greater than the transit time of the particles.
- Neutral particles only affect the expansion of plasmas with either high densities or low ionization fractions.
- Plasma detachment via three-body recombination or resistive diffusion is only relevant if significant electron cooling occurs in the plume.
- Except for low magnetic field plasmas ($B \sim 0.01T$), detachment via gradual demagnetization is unlikely.
- In the absence of electron cooling, detachment through abrupt demagnetization ($\beta_p \to 1$) and field line stretching ($\beta_k \to 1$) are predicted to occur near the same axial location.

While previous experiments have characterized many of the different ion acceleration mechanisms in nozzle-type plasma thrusters,[1,7,18,21,22] detachment of the plasma from the applied magnetic field remains relatively unstudied. Recently, plasma detachment has been observed in laboratory plasmas.[33,43,45] However, a detailed experimental investigation into the fundamental physics and scaling of plasma detachment has so far been eluded, and is crucial to the development of magnetic nozzles for propulsion applications.

References

[1]Andersen, S., Jensen, V., Nielsen, P., and D'Angelo, N., "Continuous supersonic plasma wind tunnel," *Physics Letters A*, Vol. 27, No. 8, 1968, pp. 527–528.

[2]Little, J. M. and Choueiri, E. Y., "Plasma detachment and momentum transfer in magnetic nozzles," *47th AIAA/ASME/ASEE Joint Propulsion Conference*, No. August, 2011.

[3]Podgorny, I. M. and Sagdeev, R. Z., "Physics of Interplanetary Plasma and Laboratory Experiments," *Soviet Physics Uspekhi*, Vol. 12, No. 4, April 1970, pp. 445–462.

[4]Schoenberg, K. F., Gerwin, R. a., Moses, R. W., Scheuer, J. T., and Wagner, H. P., "Magnetohydrodynamic flow physics of magnetically nozzled plasma accelerators with applications to advanced manufacturing," *Physics of Plasmas*, Vol. 5, No. 5, 1998, pp. 2090.

[5]Winglee, R., Ziemba, T., Giersch, L., Prager, J., Carscadden, J., and Roberson, B. R., "Simulation and laboratory validation of magnetic nozzle effects for the high power helicon thruster," *Physics of Plasmas*, Vol. 14, No. 6, 2007, pp. 063501.

[6]Batishchev, O. V., "Minihelicon Plasma Thruster," *IEEE Transactions on Plasma Science*, Vol. 37, No. 8, Aug. 2009, pp. 1563–1571.

[7]Longmier, B., Cassady, L., Ballenger, M., Carter, M., Chang-Díaz, F., Glover, T., Ilin, A., McCaskill, G., Olsen, C., Squire, J., and Others, "VX-200 Magnetoplasma Thruster Performance Results Exceeding Fifty-Percent Thruster Efficiency," *Journal of Propulsion and Power*, Vol. 27, No. 4, 2011.

[8]Chen, F. F., *Introduction to plasma physics and controlled fusion. Volume 1, Plasma physics*, Springer, 2nd ed., 1984.

[9]Anders, A., *A Formulary for Plasma Physics*, Berlin, Germany, 1st ed., 1990.

[10]Bering III, E., Diaz, F., Squire, J., Glover, T., Carter, M., McCaskill, G., Longmier, B., Brukardt, M., Chancery, W., and Jacobson, V., "Observations of single-pass ion cyclotron heating in a trans-sonic flowing plasma," *Physics of Plasmas*, Vol. 17, 2010, pp. 043509.

[11]Spektor, R. and Choueiri, E., "Ion acceleration by beating electrostatic waves: Domain of allowed acceleration," *Physical Review E*, Vol. 69, No. 4, April 2004, pp. 1–9.

[12]Jorns, B. and Choueiri, E., "Ion Heating with Beating Electrostatic Waves," *Physical Review Letters*, Vol. 106, No. 8, Feb. 2011, pp. 2–5.

[13]Comfort, R., "The magnetic mirror force in plasma fluid models," *Modeling magnetospheric plasma*, 1988, pp. 51–53.

[14]Arefiev, A. V. and Breizman, B. N., "Ambipolar acceleration of ions in a magnetic nozzle," *Physics of Plasmas*, Vol. 15, No. 4, 2008, pp. 042109.

[15]Arefiev, A. V. and Breizman, B. N., "Collisionless plasma expansion into vacuum: Two new twists on an old problem," *Physics of Plasmas*, Vol. 16, No. 5, 2009, pp. 055707.

[16]Saka, O., "Plasma flow characteristics in converging field line geometry in anisotropic plasmas," *Advances in polar upper atmosphere research*, 2005, pp. 80–83.

[17]Boswell, R., "Plasma production using a standing helicon wave," *Physics Letters A*, Vol. 33, No. 7, 1970, pp. 457–458.

[18]Charles, C. and Boswell, R., "Current-free double-layer formation in a high-density helicon discharge," *Applied Physics Letters*, Vol. 82, No. 9, 2003, pp. 1356.

[19]West, M. D., Charles, C., and Boswell, R. W., "Testing a Helicon Double Layer Thruster Immersed in a Space-Simulation Chamber," *Journal of Propulsion and Power*, Vol. 24, No. 1, Jan. 2008, pp. 134–141.

[20]Popov, O. a., "Characteristics of electron cyclotron resonance plasma sources," *Journal of Vacuum Science & Technology A: Vacuum, Surfaces, and Films*, Vol. 7, No. 3, May 1989, pp. 894.

[21]Kuriki, K. and Okada, O., "Experimental Study of a Plasma Flow in a Magnetic Nozzle," *Physics of Fluids*, Vol. 13, 1970, pp. 2262.

[22]Cohen, S. a., Siefert, N. S., Stange, S., Boivin, R. F., Scime, E. E., and Levinton, F. M., "Ion acceleration in plasmas emerging from a helicon-heated magnetic-mirror device," *Physics of Plasmas*, Vol. 10, No. 6, 2003, pp. 2593.

[23]Longmier, B., Bering, E., Carter, M., Cassady, L., Chancery, W., Díaz, F., Glover, T., Hershkowitz, N., Ilin, A., McCaskill, G., and Others, "Ambipolar ion acceleration in an expanding magnetic nozzle," *Plasma Sources Science and Technology*, Vol. 20, 2011, pp. 015007.

[24]Fruchtman, A., "The thrust of a collisional-plasma source," *Plasma Science, IEEE Transactions on*, Vol. 39, No. 99, 2011, pp. 1–10.

[25]Lotz, W., "Electron-impact ionization cross-sections and ionization rate coefficients for atoms and ions," *The Astrophysical Journal Supplement Series*, Vol. 14, 1967, pp. 207.

[26]Block, L. P., "A double layer review," *Astrophysics and Space Science*, Vol. 55, No. 1, 1978, pp. 59–83.

[27]Ahedo, E., "Double-layer formation and propulsive assessment for a three-species plasma expanding in a magnetic nozzle," *Physics of Plasmas*, Vol. 18, No. 3, 2011, pp. 033510.

[28]Cohen, S. and Paluszek, M. A., "The Grand Challenge: A New Plasma Thruster," *Launchspace*, 1998, pp. 46–50.

[29]Dimov, G. I. and Taskaev, S. Y., "Simulation of a supersonic plasma jet with recombination in a magnetic nozzle," *27th EPS Conference on Contr. Fusion and Plasma Phys.*, Vol. 24, 2000, pp. 464–467.

[30]Moses Jr, R., Gerwin, R., and Schoenberg, K., "Resistive plasma detachment in nozzle based coaxial thrusters," *AIP Conference Proceedings*, Vol. 246, 1992, p. 1293.

[31]Hooper, E., "Plasma detachment from a magnetic nozzle," *Journal of Propulsion and Power*, Vol. 9, No. 5, 1993, pp. 757–763.

[32]Merino, M. and Ahedo, E., "Plasma detachment mechanisms in a magnetic nozzle," *47th AIAA/ASME/ASEE Joint Propulsion Conference*, No. 3, 2011, pp. 1–11.

[33]Terasaka, K., Yoshimura, S., Ogiwara, K., Aramaki, M., and Tanaka, M. Y., "Experimental studies on ion acceleration and stream line detachment in a diverging magnetic field," *Physics of Plasmas*, Vol. 17, No. 7, 2010, pp. 072106.

[34]Ahedo, E. and Merino, M., "Two-dimensional supersonic plasma acceleration in a magnetic nozzle," *Physics of Plasmas*, Vol. 17, No. 1, 2010, pp. 1–16.

[35]Lorzel, H. and Mikellides, P. G., "Three-Dimensional Modeling of Magnetic Nozzle Processes," *AIAA Journal*, Vol. 48, No. 7, July 2010, pp. 1494–1503.

[36]Sankaran, K. and Polzin, K. A., "Numerical Investigation of Near-Field Plasma Flows in Magnetic Nozzles," *AIAA Joint Propulsion Conference*, No. August, 2009.

[37]Roberson, B. R., Winglee, R., and Prager, J., "Enhanced diamagnetic perturbations and electric currents observed downstream of the high power helicon," *Physics of Plasmas*, Vol. 18, No. 5, 2011, pp. 053505.

[38]Arefiev, A. V. and Breizman, B. N., "Magnetohydrodynamic scenario of plasma detachment in a magnetic nozzle," *Physics of Plasmas*, Vol. 12, No. 4, 2005, pp. 043504.

[39]Breizman, B. N., Tushentsov, M. R., and Arefiev, a. V., "Magnetic nozzle and plasma detachment model for a steady-state flow," *Physics of Plasmas*, Vol. 15, No. 5, 2008, pp. 057103.

[40]Little, J. M. and Choueiri, E. Y., "The Influence of Induced Currents on Magnetic Nozzle Acceleration and Plasma Detachment," *46th AIAA Joint Propulsion Conference*, Nashville, Tn, 2010, pp. 1–14.

[41]Chubb, D., "Fully ionized quasi-one-dimensional magnetic nozzle flow," *AIAA Journal*, 1972.

[42]York, T., Mikellides, P., and Jacoby, B., "Plasma flow processes within magnetic nozzle configurations," *Journal of Propulsion and Power*, 1992.

[43]Deline, C. a., Bengtson, R. D., Breizman, B. N., Tushentsov, M. R., Jones, J. E., Chavers, D. G., Dobson, C. C., and Schuettpelz, B. M., "Plume detachment from a magnetic nozzle," *Physics of Plasmas*, Vol. 16, No. 3, 2009, pp. 033502.

[44]Fiksel, G., Craig, D., Hartog, D., Holly, D., Kendrick, R., Lovell, T., Oliva, S., Prager, S., Sarff, J., and Thomas, M., "High current plasma electron emitter," *IEEE Conference Record - Abstracts. 1996 IEEE International Conference on Plasma Science*, Vol. 78, 1996, pp. 219.

[45]Takahashi, K., Itoh, Y., and Fujiwara, T., "Operation of a permanent-magnets- expanding plasma source connected to a large-volume diffusion chamber," *Journal of Physics D: Applied Physics*, Vol. 44, No. 1, Jan. 2011, pp. 015204.

[46]Rynn, N. and D'Angelo, N., "Device for Generating a Low Temperature, Highly Ionized Cesium Plasma," *Review of Scientific Instruments*, Vol. 31, No. 12, 1960, pp. 1326.

[47]Hopwood, J., "Review of inductively coupled plasmas for plasma processing," *Plasma Sources Science and Technology*, Vol. 1, 1992, pp. 109.

[48]Scime, E. E., Keiter, P. a., Zintl, M. W., Balkey, M. M., Kline, J. L., and Koepke, M. E., "Control of ion temperature anisotropy in a helicon plasma," *Plasma Sources Science and Technology*, Vol. 7, No. 2, May 1998, pp. 186–191.

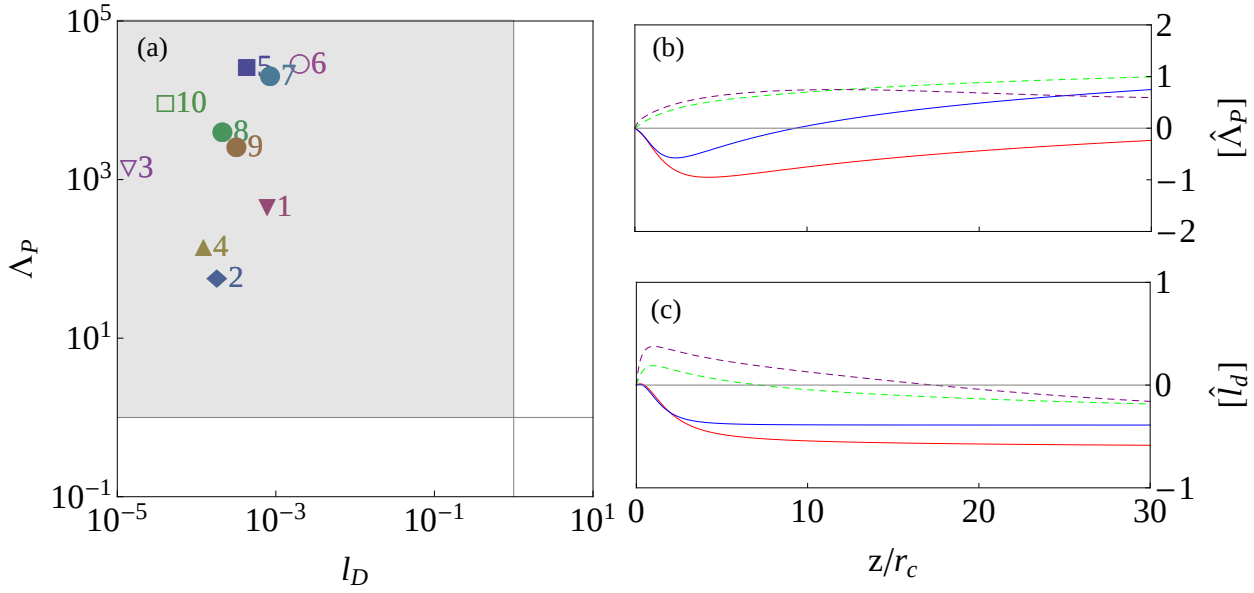

Figure 2. Plasma Quality: (a) Normalized Debye length, l_D, and plasma parameter, Λ_P, for the experiments shown in Table I; Axial evolution of the (b) plasma parameter and (c) normalized Debye length. Each parameter is presented in the form: $[\hat{X}] = \log_{10}(X/X_0)$, where X_0 is the value at the throat ($z = 0$). Lines represent solutions with the following properties: isothermal electrons (solid red) $\gamma_e = 1$, $\Theta_{eq,0} = 10^5$, $\Theta_{iso,0} = 1$; isentropic electrons (solid blue) $\gamma_e = 5/3$, $\Theta_{eq,0} = 10^{-4}$, $\Theta_{iso,0} = 1$; cold electrons, anisotropic ions (dashed green) $\gamma_e = 1.2$, $\Theta_{eq,0} = 0$, $\Theta_{iso,0} = 10$; cold electrons, anisotropic ions (dashed purple) $\gamma_e = 1.2$, $\Theta_{eq,0} = 0$, $\Theta_{iso,0} = 100$

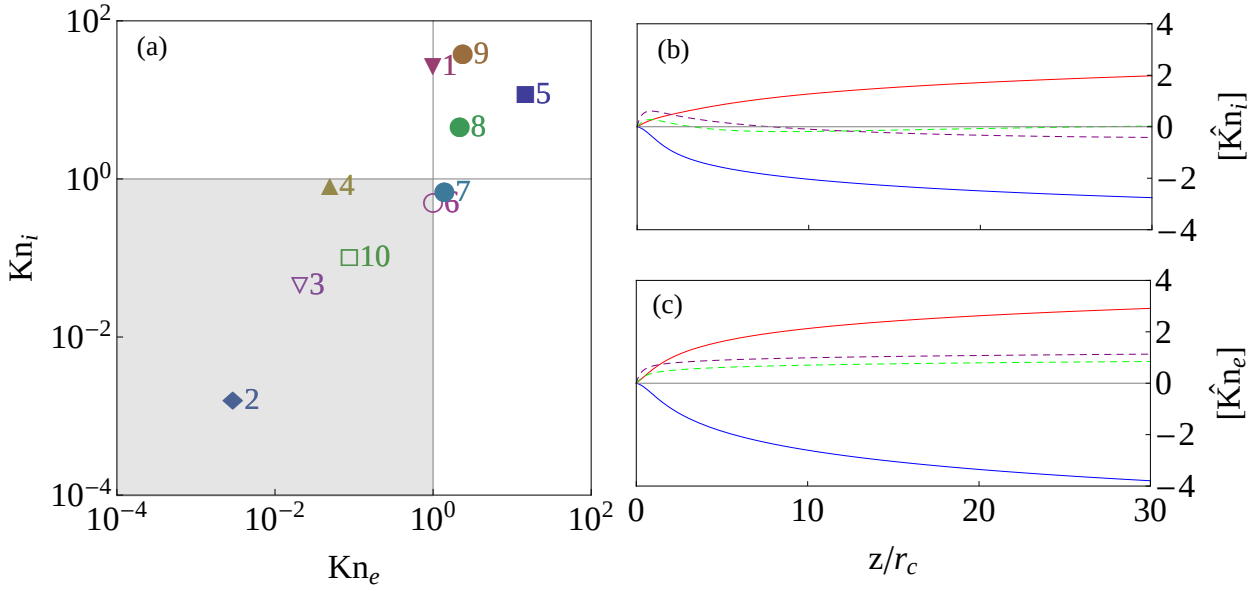

Figure 3. Plasma Quality: (a) Electron Knudsen number, Kn_e, and ion Knudsen number, Kn_i, for the experiments shown in Table I; Axial evolution of the (b) ion Knudsen number and (c) electron Knudsen number. Each parameter is presented in the form: $[\hat{X}] = \log_{10}(X/X_0)$, where X_0 is the value at the throat ($z = 0$). Lines represent solutions with the following properties: isothermal electrons (solid red) $\gamma_e = 1$, $\Theta_{eq,0} = 10^5$, $\Theta_{iso,0} = 1$; isentropic electrons (solid blue) $\gamma_e = 5/3$, $\Theta_{eq,0} = 10^{-4}$, $\Theta_{iso,0} = 1$; cold electrons, anisotropic ions (dashed green) $\gamma_e = 1.2$, $\Theta_{eq,0} = 0$, $\Theta_{iso,0} = 10$; cold electrons, anisotropic ions (dashed purple) $\gamma_e = 1.2$, $\Theta_{eq,0} = 0$, $\Theta_{iso,0} = 100$

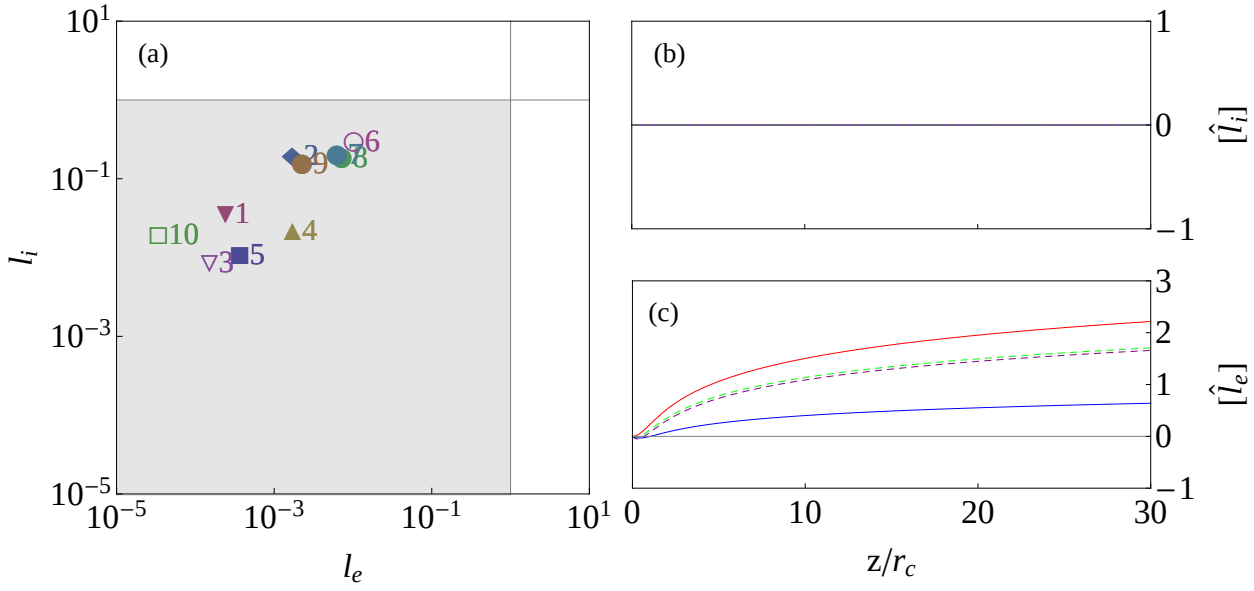

Figure 4. Confinement: (a) Normalized electron Larmor radius, l_e, and ion Larmor radius, l_i, for the experiments shown in Table I; Axial evolution of the normalized (b) ion and (c) electron Larmor radii. Each parameter is presented in the form: $[\hat{X}] = \log_{10}(X/X_0)$, where X_0 is the value at the throat ($z = 0$). Lines represent solutions with the following properties: isothermal electrons (solid red) $\gamma_e = 1$, $\Theta_{eq,0} = 10^5$, $\Theta_{iso,0} = 1$; isentropic electrons (solid blue) $\gamma_e = 5/3$, $\Theta_{eq,0} = 10^{-4}$, $\Theta_{iso,0} = 1$; cold electrons, anisotropic ions (dashed green) $\gamma_e = 1.2$, $\Theta_{eq,0} = 0$, $\Theta_{iso,0} = 10$; cold electrons, anisotropic ions (dashed purple) $\gamma_e = 1.2$, $\Theta_{eq,0} = 0$, $\Theta_{iso,0} = 100$

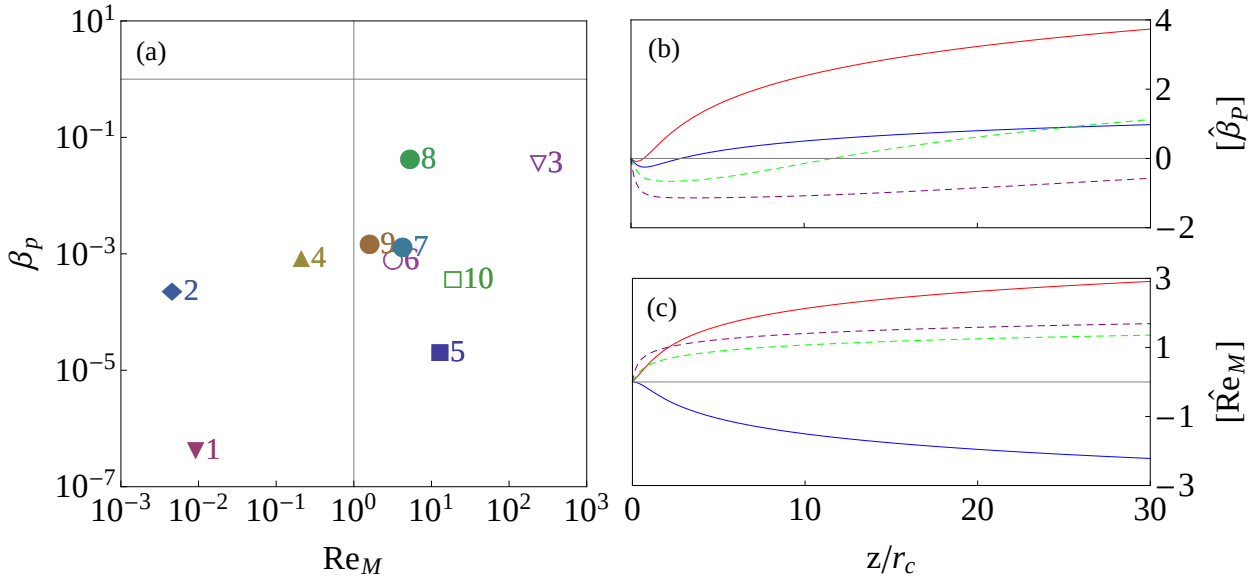

Figure 5. Confinement: (a) Magnetic Reynolds number, Re_M, and plasma-beta, β_p, for the experiments shown in Table I; Axial evolution of the (b) magnetic Reynolds number and (c) plasma-beta. Each parameter is presented in the form: $[\hat{X}] = \log_{10}(X/X_0)$, where X_0 is the value at the throat ($z = 0$). Lines represent solutions with the following properties: isothermal electrons (solid red) $\gamma_e = 1$, $\Theta_{eq,0} = 10^5$, $\Theta_{iso,0} = 1$; isentropic electrons (solid blue) $\gamma_e = 5/3$, $\Theta_{eq,0} = 10^{-4}$, $\Theta_{iso,0} = 1$; cold electrons, anisotropic ions (dashed green) $\gamma_e = 1.2$, $\Theta_{eq,0} = 0$, $\Theta_{iso,0} = 10$; cold electrons, anisotropic ions (dashed purple) $\gamma_e = 1.2$, $\Theta_{eq,0} = 0$, $\Theta_{iso,0} = 100$

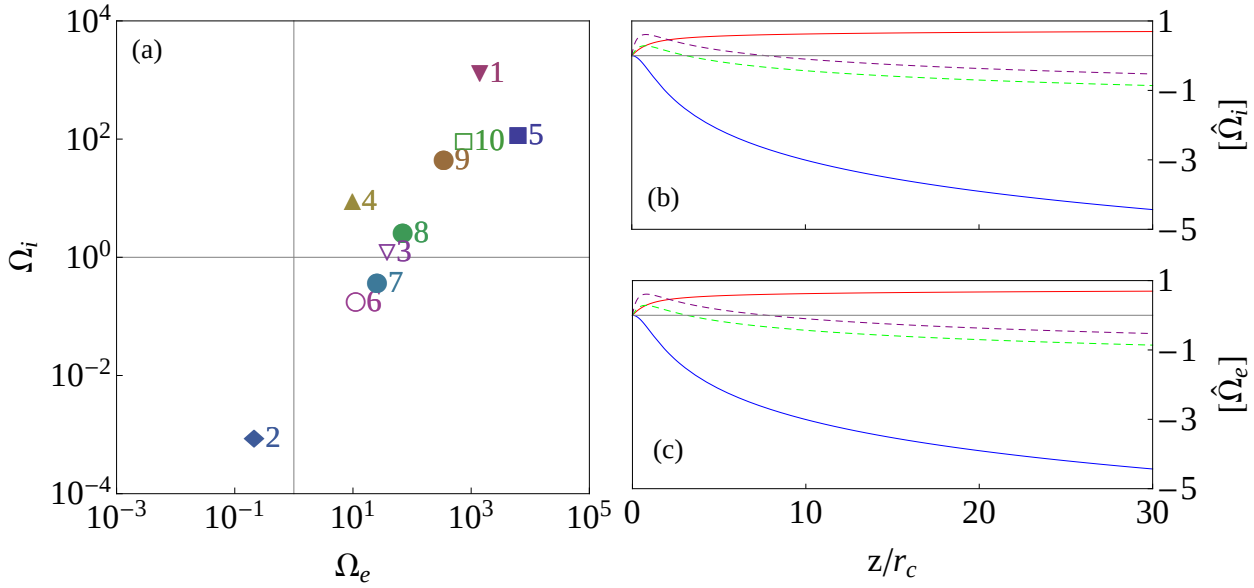

Figure 6. Confinement: (a) Electron Hall parameter, Ω_e, and ion Hall parameter, Ω_i, for the experiments shown in Table I; Axial evolution of the (b) ion and (c) electron Hall parameters. Each parameter is presented in the form: $[\hat{X}] = \log_{10}(X/X_0)$, where X_0 is the value at the throat ($z = 0$). Lines represent solutions with the following properties: isothermal electrons (solid red) $\gamma_e = 1$, $\Theta_{eq,0} = 10^5$, $\Theta_{iso,0} = 1$; isentropic electrons (solid blue) $\gamma_e = 5/3$, $\Theta_{eq,0} = 10^{-4}$, $\Theta_{iso,0} = 1$; cold electrons, anisotropic ions (dashed green) $\gamma_e = 1.2$, $\Theta_{eq,0} = 0$, $\Theta_{iso,0} = 10$; cold electrons, anisotropic ions (dashed purple) $\gamma_e = 1.2$, $\Theta_{eq,0} = 0$, $\Theta_{iso,0} = 100$

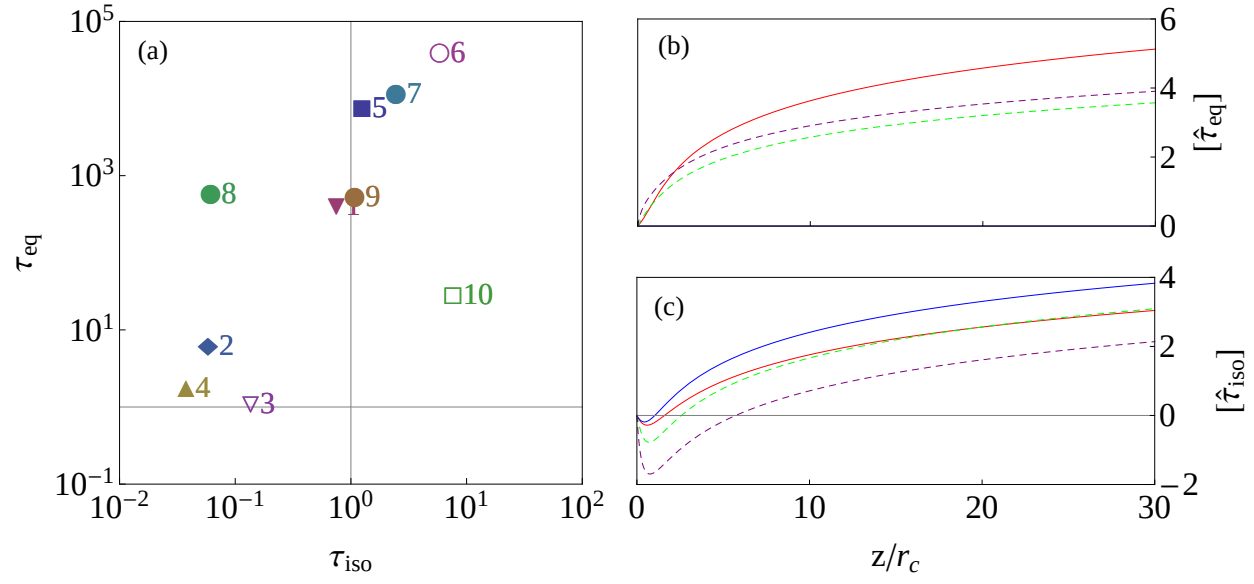

Figure 7. Acceleration: (a) Ion temperature isotropization parameter, τ_{iso}, and species equilibration parameter, τ_{eq}, for the experiments shown in Table I; Axial evolution of the (b) equilibration parameter (c) isotropization parameter. Each parameter is presented in the form: $[\hat{X}] = \log_{10}(X/X_0)$, where X_0 is the value at the throat ($z = 0$). Lines represent solutions with the following properties: isothermal electrons (solid red) $\gamma_e = 1$, $\Theta_{eq,0} = 10^5$, $\Theta_{iso,0} = 1$; isentropic electrons (solid blue) $\gamma_e = 5/3$, $\Theta_{eq,0} = 10^{-4}$, $\Theta_{iso,0} = 1$; cold electrons, anisotropic ions (dashed green) $\gamma_e = 1.2$, $\Theta_{eq,0} = 0$, $\Theta_{iso,0} = 10$; cold electrons, anisotropic ions (dashed purple) $\gamma_e = 1.2$, $\Theta_{eq,0} = 0$, $\Theta_{iso,0} = 100$

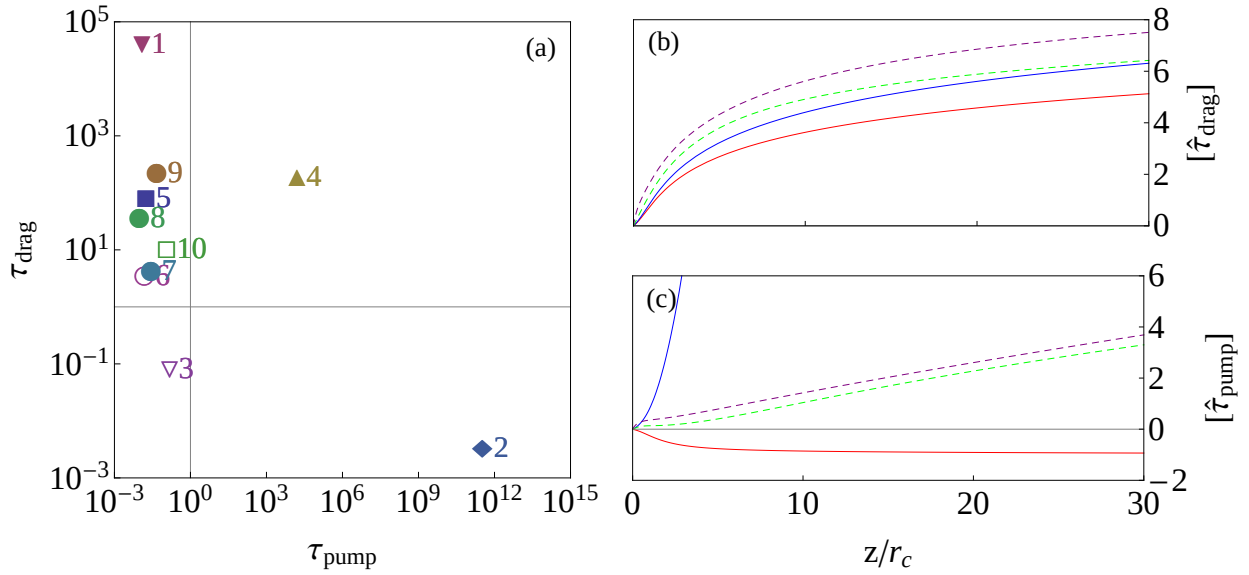

Figure 8. Acceleration: (a) Neutral pumping parameter, τ_{pump}, and neutral drag parameter, τ_{drag}, for the experiments shown in Table I; Axial evolution of the (b) neutral pumping parameter and (c) neutral drag parameter. Each parameter is presented in the form: $[\hat{X}] = \log_{10}(X/X_0)$, where X_0 is the value at the throat ($z = 0$). Lines represent solutions with the following properties: isothermal electrons (solid red) $\gamma_e = 1$, $\Theta_{eq,0} = 10^5$, $\Theta_{iso,0} = 1$; isentropic electrons (solid blue) $\gamma_e = 5/3$, $\Theta_{eq,0} = 10^{-4}$, $\Theta_{iso,0} = 1$; cold electrons, anisotropic ions (dashed green) $\gamma_e = 1.2$, $\Theta_{eq,0} = 0$, $\Theta_{iso,0} = 10$; cold electrons, anisotropic ions (dashed purple) $\gamma_e = 1.2$, $\Theta_{eq,0} = 0$, $\Theta_{iso,0} = 100$

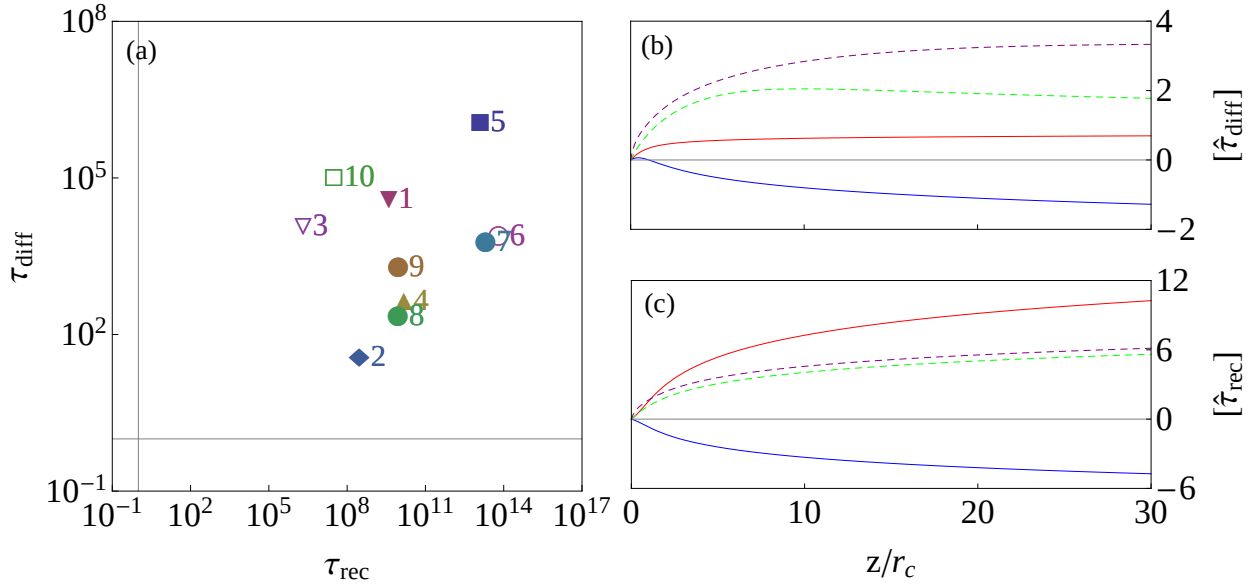

Figure 9. Detachment: (a) Three-body recombination parameter, τ_{rec}, and cross-field diffusion parameter, τ_{diff}, for the experiments shown in Table I; Axial evolution of the (b) three-body recombination and (c)cross-field diffusion parameters. Each parameter is presented in the form: $[\hat{X}] = \log_{10}(X/X_0)$, where X_0 is the value at the throat ($z = 0$). Lines represent solutions with the following properties: isothermal electrons (solid red) $\gamma_e = 1$, $\Theta_{eq,0} = 10^5$, $\Theta_{iso,0} = 1$; isentropic electrons (solid blue) $\gamma_e = 5/3$, $\Theta_{eq,0} = 10^{-4}$, $\Theta_{iso,0} = 1$; cold electrons, anisotropic ions (dashed green) $\gamma_e = 1.2$, $\Theta_{eq,0} = 0$, $\Theta_{iso,0} = 10$; cold electrons, anisotropic ions (dashed purple) $\gamma_e = 1.2$, $\Theta_{eq,0} = 0$, $\Theta_{iso,0} = 100$

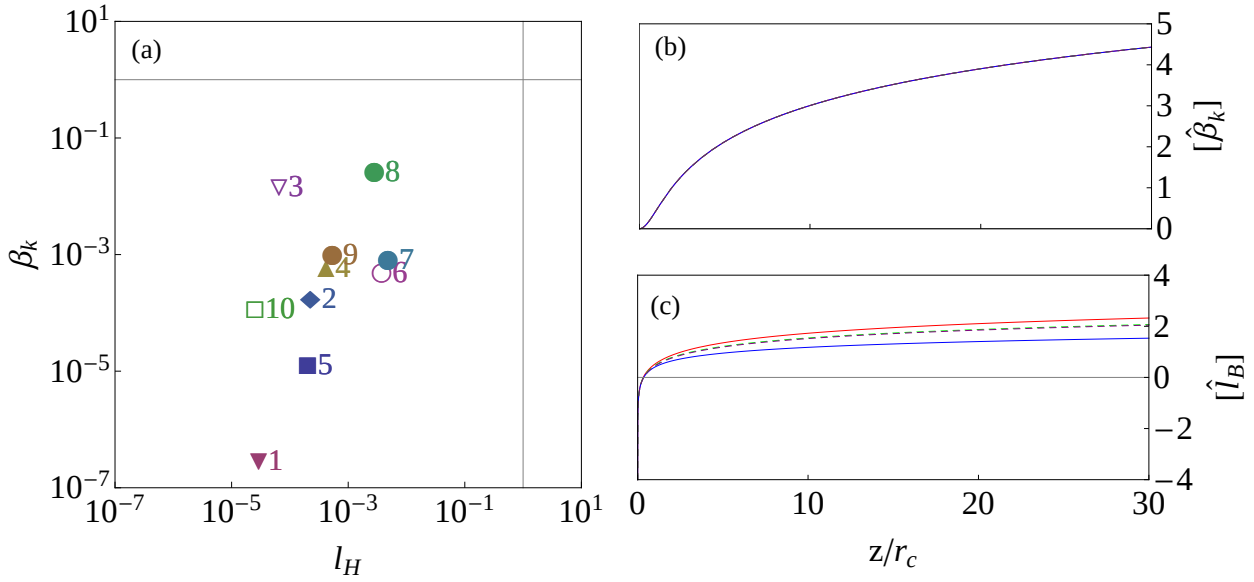

Figure 10. Detachment: (a) Normalized hybrid Larmor radius, l_H, and dynamic plasma-beta, β_k, for the experiments shown in Table I; Axial evolution of the (b) magnetization parameter, $\hat{l}_B$, and (c) dynamic plasma-beta. Each parameter is presented in the form: $[\hat{X}] = \log_{10}(X/X_0)$, where X_0 is the value at the throat ($z = 0$). Lines represent solutions with the following properties: isothermal electrons (solid red) $\gamma_e = 1$, $\Theta_{eq,0} = 10^5$, $\Theta_{iso,0} = 1$; isentropic electrons (solid blue) $\gamma_e = 5/3$, $\Theta_{eq,0} = 10^{-4}$, $\Theta_{iso,0} = 1$; cold electrons, anisotropic ions (dashed green) $\gamma_e = 1.2$, $\Theta_{eq,0} = 0$, $\Theta_{iso,0} = 10$; cold electrons, anisotropic ions (dashed purple) $\gamma_e = 1.2$, $\Theta_{eq,0} = 0$, $\Theta_{iso,0} = 100$